A New Albite Microanalytical Reference Material from Piz Beverin for Na, Al and Si Determination, and the Potential for New K-Feldspar Reference Materials

Julien M. **Allaz** (1)* iD, Marcel **Guillong** (1), Lorenzo **Tavazzani** (1), Georg **Spiekermann** (1), Lydia **Zehnder** (1), Emma **Bullock** (2), Joel **DesOrmeau** (3), Michael J. **Jercinovic** (4), Joachim **Krause** (5), Felix **Marxer** (6) iD, William O. **Nachlas** (7) and John **Spratt** (8)

(1) Department of Earth Sciences, Institute of Geochemistry and Petrology, ETH Zürich, Clausiusstrasse 25, 8092 Zürich, Switzerland
(2) Carnegie Science, Earth and Planets Laboratory, 5241 Broad Branch Road, NW, Washington, DC 20015, USA
(3) Reno, Department of Geological Sciences and Engineering, University of Nevada, 1664 N. Virginia Street, Reno, NV 89557-0172, USA
(4) 154 Morrill Science Center, Department of Geosciences, University of Massachusetts, 01003 Amherst, USA
(5) Helmholtz-Zentrum Dresden-Rossendorf, Helmholtz Institute Freiberg for Resource Technology, Chemnitzer Strasse 40,09599 Freiberg, Germany
(6) Institute of Mineralogy, Leibniz University Hannover, Callinstrasse 3, 30167 Hannover, Germany
(7) Madison, Department of Geoscience, University of Wisconsin, 1215 West Dayton Street, Madison, WI 53706, USA
(8) The Natural History Museum, Core Research Laboratories, Cromwell Road, London SW7 5BD, UK
* Corresponding author. e-mail: julien.allaz@erdw.ethz.ch

Determination of alkali elements is important to Earth scientists, yet suitable and reliable microanalytical reference materials are lacking. This paper proposes a new albite reference material and evaluates the potential for future K-feldspar reference materials. The proposed Piz Beverin albite reference material from Switzerland yields a homogeneous composition at the centimetre- to micrometre-scale for Si, Al and Na with < 2000 µg g^{-1} total trace elements (mostly heterogeneously distributed Ca, K and Sr). EPMA and LA-ICP-MS measurements confirm a composition of 99.5(2)% albite component, which is supported further by bulk XRF measurements. A round robin evaluation involving nine independent EPMA laboratories confirms its composition and homogeneity for Si, Al and Na. In addition, a set of five distinct clear K-feldspar samples was evaluated as possible reference materials. The first two crystals of adular and orthoclase yield unacceptable inhomogeneities with $> 2\%$ relative local variations of Na, K and Ba contents. The three other investigated sets of K-feldspar crystals are yellow sanidine crystals from Itrongay (Madagascar). Despite distinct compositions, EPMA confirms they are each homogeneous at the centimetre to micrometre scale for Si, Al and K and have no apparent inclusions; further investigation to find larger amounts of these materials is therefore justified.

Keywords: natural microanalytical reference materials, alkali elements, feldspar minerals, RM evaluation, combined EPMA, LA-ICP-MS and XRF analysis.

High-quality microanalytical reference materials (µRM) are necessary for the calibration and quality control of quantitative X-ray analysis for major and minor elements at the (sub-)micrometre scale with an electron probe micro-analyser (EPMA) or scanning electron microscope (SEM) equipped with wavelength dispersive (WD) or energy dispersive (ED) spectrometers. The microanalytical community requires high quality µRM that are available indefinitely at little or no cost. The challenge is therefore to find a µRM that:

(1) is available in sufficient quantity (for natural samples) or is reproducible (for synthetic materials),
(2) has a suitable grain size for microanalysis (ideally > 100 µm),

(3) has a homogeneous and well-characterised reference composition for major elements that ideally can be certified or supported by independent laboratories and methods,

(4) has a thorough accounting of possible contaminants such as in trace elements, presence of element impurities, or other inclusions of other phases,

(5) is easy to prepare, polish and maintain,

(6) is stable over time, under vacuum and under the electron beam (within reason), and

(7) with either a complete recipe for synthesised material or, if the proposed μRM is natural, a precise location for possible batch identification, and future re-sampling and re-certification.

Several simple materials such as oxides can be easily synthesised in large quantities and at a good homogeneity level with only trace impurities in the hundreds of μg g^{-1} range or below (e.g., MgO, Al$_2$O$_3$, SiO$_2$, Fe$_x$O$_y$). These thus provide an excellent and simple μRM for several elements. Unfortunately, these materials do not account for all the analytes that could be of interest. For elements such as Na and K, which are of great importance to earth scientists, μRM's that meet the above criteria regarding purity and homogeneity are, at this time, either too difficult or too expensive to synthesise in sufficient quantities to be of use to the wider community. Several easily prepared synthetic and pure Na- or K-rich materials exist (e.g., chloride, fluoride, borate). These, however, are not optimal due to (1) their very different matrix compositions compared with the unknowns, and (2) their obvious sample preparation difficulties: easily soluble in water or alcohol, difficult to polish, prone to damage during electron beam exposure, etc. Similarly, alkali-rich Si- and Al-fluorides are unstable under the electron beam, and they remain an imperfect matrix match to an alkali-silicate. Sodium- and/or K-rich silicate glasses exist, yet they still suffer from instability under the electron beam, and some are prone to devitrification problems (e.g., USNM 113716 basaltic glass; P. Carpenter, U. of Oregon EPMA workshop 2010 and pers. comm.). Ito and Frondel (1968) suggested the synthesis of a scandium analogue of pyroxene: NaScSi$_2$O$_6$. Although this could be a suitable μRM for Na in silicate, it remains to be tested, and it should be emphasised that the mass absorption coefficient (MAC) of Sc over Na $K\alpha$ (~ 4550; Chantler et al. 2005) is 3.5 or 4.6 times larger than the MAC of Na $K\alpha$ from Si (~ 1312) or Al (~ 985). With the X-ray fluorescence yield of Na $K\alpha$ already being low, this high MAC would further add uncertainty on the Na-measurement in the μRM by lowering the X-ray count-rate on the ED or WD detector (lowering precision) as well as increasing dependence on matrix corrections (lowering accuracy).

Natural Na- and K-silicates also exist, and they have their own benefits and drawbacks. For instance, K- or Na-micas form very thin flakes in the 1–100 μm range; these sheets can be quite homogeneous, but they are very difficult to prepare, polish, and maintain over years for microanalytical work. Sodium-rich pyroxenes (e.g., jadeite, omphacite) are known to be quite heterogeneous, and amphiboles rarely contain a high enough alkali content suitable for calibration of Na and K as a major element in the unknown sample. Natural sodalite-group minerals such as tugtupite or sodalite (ideally: Na$_4$BeAlSi$_4$O$_{12}$Cl or Na$_4$Al$_3$Si$_3$O$_{12}$Cl) are available from vendors, but they usually come with a potentially questionable (and uncertified) "reference" composition, although with a community effort this could be improved. Ribbe and Smith (1966) and Smith and Ribbe (1966) were among the first one to perform detailed microanalyses of a large variety of plagioclase and alkali-feldspar minerals to evaluate possible μRM. C.O. Ingamells evaluated potential microprobe reference materials in his microprobe column in the Geostandards Newsletter (1979–1981), including Na and K-bearing phases such as sodalite (Ingamells 1981a), biotite (Ingamells 1981b) and K-feldspar (Ingamells 1981c), the results of which remained somewhat pessimistic. Eugene Jarosewich from the Smithsonian Institution (USA) provided the community with a large set of μRM (Jarosewich et al. 1980, Jarosewich 2002). Unfortunately, this collection does not contain any Na-rich phases. Moreover, the few Na- or K-bearing phases available have known issues, for instance (a) the Kakanui hornblende NMHN 143965 has inclusions of melt and titanomagnetite detected at the sub-micrometre scale (Vicenzi and Rose 2008, Carpenter and Vicenzi 2012), and (b) investigation of a nine-grain mount NMNH 143966 microcline at ETH revealed grain-to-grain variations, with one grain yielding significantly higher K-content and lower Na-content at 0.980 X_K (= K / Ca + Na + K + Ba [atomic]) compared with the usual 0.880 X_K of this μRM. When it comes to natural samples, an apparently "good" μRM can quickly become a "bad" one (following the nomenclature of Carpenter 2008) when significant heterogeneities, impurities, or other problems are identified. The community deserves better quality assessment of its synthetic and natural μRM (Bullock et al. 2021).

Ideal crystalline (Na, K) μRM are found in the feldspar-group end members: albite and K-feldspar (with its polymorph orthoclase, sanidine and microcline). High-purity albite (ideally NaAlSi$_3$O$_8$) is difficult to synthesise in large quantities, yet it can be abundant in nature, notably in pegmatites and in greenschist facies metamorphic rocks. However, purity and homogeneity are questionable. Natural feldspar μRMs are commonly available under the label

"albite" (for instance), but their exact origin and quality remain commonly obscure with one or more of the following impediments:

- lack of acceptably documented reference composition,

- an assumed perfect stoichiometry,

- mistakes in the list of reference values,

- no assessment of homogeneity at the micrometre-scale,

- no uncertainty report on the data,

- no detail on the analytical technique used for the reference analysis,

- no exact provenance for the natural sample.

Table 1 is a compilation of some reference compositions for albite and K-feldspar μRM. Some μRM holding the same name, such as "Amelia albite", show variability in their absolute reference weight-% data stored in each laboratory, which either stem from distinct sample location and small natural variabilities, or from different reference compositions given by the provider, or even sometimes from "adjustments" by the individual laboratories. Moreover, none of these RM data come with a certified analysis with proper analytical uncertainty. Such inter-laboratory variation for the same RM material can be in the order of 1% relative on the weight per cent value, which can potentially translate into an inaccuracy error of up to 1% when considering the values for the Amelia albite RM in Table 1. USGS at Reston evaluated their μRM, including an albite from Tiburon peninsula (CA, USA; Huebner and Woodruff 1985), which is the albite standard currently in use at ETH Zürich for Si and Na calibration of most silicates.

This paper aims to provide a detailed investigation of an albite mineral stemming from an open fracture near "Piz Beverin" in Switzerland. This sample is proposed as a μRM for Si, Na and Al. Major and trace element compositions are evaluated with multiple instruments, notably SEM for SE, BSE and CL imaging, and quantitative analyses by SEM-ED, EPMA, LA-ICP-MS and XRF. Nine independent EPMA laboratories assessed the composition and homogeneity by analysing multiple batches and grains. This material appears to be an excellent μRM for quantitative X-ray microanalysis by EPMA or SEM (WD or ED), micro-XRF, or any other microanalytical techniques for Na, Si, or Al measurement. Each centimetre-sized albite crystal is homogeneous at the micrometre-scale and the material is available in significant quantities (> 100 g).

In parallel, a set of two clear and three yellow K-feldspar minerals from the ETH Zürich collection, all of gem-quality, was investigated by EPMA and one by LA-ICP-MS. The two clear K-feldspar samples show heterogeneities in K, Na, Ba and/or Fe, making them unsuitable for microanalytical reference materials. On the contrary, each individual set of yellow Madagascar K-feldspar shows excellent homogeneity, yet each with distinct and well defined Si, Al and K contents.

Sample presentation

Piz Beverin albite (PB Ab)

The investigated albite sample originates from the museum collection of the Earth Sciences department at ETH Zürich and was provided by Dr. Peter Brack and Dr. Andrea Galli (initially donated to the collection by an unknown mineral collector). According to its handwritten museum note, this sample was collected on the NE side of the summit "Piz Beverin" (PB), SW of the locality of Flerden near Thusis (canton Graubünden, Switzerland; 46°40'20.3" North, 9°22'55.5" East; Figure 1). The sample was taken from an open-fracture within the graphitic-schist rocks of the Tomül nappe (Nolla schist) in the lower Penninic nappe (Wyss and Wiederkehr 2017; Figure 1).

The original set of PB albite consisted of four large samples (~ 5 × 5 × 8 cm), six smaller pieces (~ 2 × 2 × 4 cm), and some loose material, all originating from the same outcrop. All fragments are milky to translucent albite crystals with a small portion of the host rock (Nolla schist) attached to the base. Individual macroscopic albite crystals have a platy aspect and range in size from ~ 0.5 cm to 5 cm in width and height and up to ~ 1 cm in thickness (mostly below 0.5 cm; Figure 2a, b). The base (core) of each individual albite crystal is commonly milky-white, whereas the top part (rim) tends to be more translucent to clear. The idiomorphic albite crystals are recognisable by their tabular aspect and their pronounced cleavage. Rare glass-clear crystals with typical trigonal habit or conchoidal fractures are identified as quartz.

K-feldspar minerals

Five different K-feldspar crystal sets found in the ETH mineral collection were evaluated. They originate from the potential set of μRM for SEM-ED and EPMA-WD left by Dr. Eric Reusser (ETH Zürich; now retired). All investigated K-feldspar crystals are idiomorphic, clear, without any optically

GEOSTANDARDS and GEOANALYTICAL RESEARCH

Table 1.

Compilation of some commonly used Na and K feldspar micro reference materials in SEM and EPMA laboratories

(a) Some albite RMs used in other laboratories or sold by private companies

Mineral	Amelia Courthouse (VA, USA) albite					
Code or provider	AS5020	CM Taylor	Astimex	P&H	-	Cannon Microprobe
Data source	SPI, CM Taylor	CU Boulder (USA)	U. of Iowa (USA)	U. of Iowa (USA)	E.J. Olsen	Kurt Hollocher
Si	**31.85**	**31.85**	**32.03**	**32.10**	**32.11**	**31.95**
Al	**10.46**	**10.46**	**10.34**	**10.32**	**10.32**	**10.36**
Fe^{3+}	-	0.008	-	-	-	0.06
Ca	0.30	0.27	0.09	-	-	0.17
Na	**8.50**	**8.50**	**8.60**	**8.71**	**8.68**	**8.52**
K	0.20	0.19	0.18	0.11	0.08	0.22
O	48.70	48.70	48.76	48.76	48.80	48.72
Total	100.01	99.99	100.00	100.00	100.00	100.00

(b) Some K-feldspar RMs used in other laboratories or sold by private companies

Mineral	Microcline			Sanidine		
Code or provider	**NMNH 143966**	**Asbestos microcline**	**P-102**	**P-28**	**P-28**	**Orthoclase**
Data source	Smithsonian Institution*	E.J. Olsen	Smith and Ribbe**	Maynes and Birgham**	U. of Mass. Amherst	MicroAnalytical Consultant
Si	**30.03**	**29.87**	**30.30**	**29.85**	**30.62**	**30.06**
Al	**9.69**	**9.53**	**9.77**	**9.95**	**9.53**	**10.53**
Fe^{3+}	0.031	0.031	0.03	0.14	-	-
Ca	0.014	0.143	0.010	0.071	0.071	0.172
Na	0.96	0.07	0.97	1.83	1.67	2.75
K	**12.57**	**13.70**	**12.68**	**10.40**	**10.88**	**9.46**
Ba	-	0.09	1.04	1.04	0.99	-
Sr	-	-	0.25	0.25	-	-
Rb	-	-	-	-	-	-
O	45.77	45.41	46.34	45.87	46.31	46.57
Total	99.06	98.84	101.39	99.40	100.05	99.54

* Not listed: traces of Mg, Ti, Mn, P.
** Not listed: traces of Mg (100–200 µg g^{-1}).
[1] Huebner and Woodruff (1985)

visible inclusions, and rarely with some minor surface alteration.

Two of them are colourless and crystal-clear, and labelled respectively "Adular" (most likely from Switzerland) and "Orthoclase" (collected near Disentis, canton Graubünden, Switzerland) with little detail on their handwritten note.

The three other K-feldspar minerals are clear yellow "orthoclase" from the Itrongay pegmatite field found in the province of Anosy near Mahaso East (Madagascar; Coombs 1954): "S231", "S232" and "Peretti Kfsp". The latter was given by Adolf Peretti (GemResearch Swisslab) to Dr. Reusser. Whereas the literature and individual notes on these samples refer to these minerals as a yellow ferriferous "orthoclase", it is a monoclinic low-sanidine (Simmons and Falster 2002). Their exact sampling location in Itrongay is unknown at the time of publication, but it is very likely that all three yellow sanidine crystals stem from different pegmatite bodies or local outcrops.

Tiburon albite (USA)				Other albite minerals			
USGS Reston	-	-	-	AS1010, AS1015	-	EPS 113, Ab 42-69 Langlois	-
DB Stewart, JS Huebner[1]	ETH Zürich	U. Washington (WA, USA)	U. Michigan (MI, USA), K. Hollocher	SPI	Brammer standard	E. Ghent, R. Colemann	MicroAnalytical Consultant
32.07	**32.10**	**32.13**	**31.99**	**32.03**	**31.64**	**32.16**	**30.19**
10.27	**10.29**	**10.25**	**10.37**	**10.34**	**10.40**	**10.27**	**11.32**
-	-	0.054	-	-	0.041	0.016	-
-	-	-	0.14	0.09	0.39	0.03	1.00
8.78	**8.72**	**8.75**	**8.57**	**8.60**	**8.39**	**8.75**	**8.81**
0.017	0.025	0.025	0.19	0.18	0.11	-	0.61
48.72	48.80	48.79	48.75	48.76	48.54	48.86	48.05
99.85	99.96	100.00	100.01	100.00	99.51	100.10	99.99

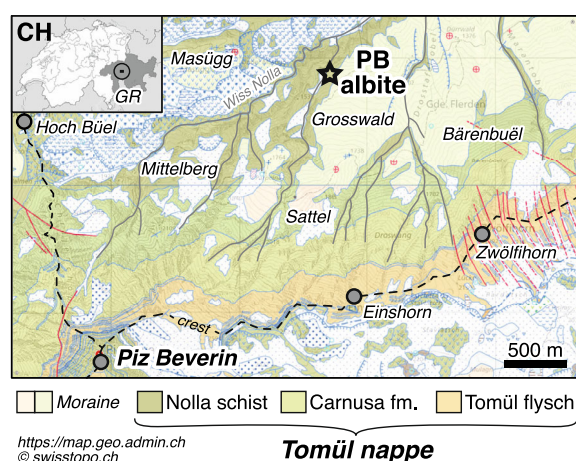| Orthoclase					K-fsp
EPS 90 Adularia Or-1 S-168	**Orthoclase, B. Evans**	**MAD-10 (Madagascar sanidine?)**	**MAD-10 (Madagascar sanidine?)**	**CM. Taylor (Madagascar sanidine?)**	**-**
Ed Ghent, N. Suhr	Ingamells	CM Taylor	U. Washington (WA, USA)	SPI	Brammer standard
30.10	**30.10**	**30.29**	**30.22**	**30.23**	**31.31**
9.83	**9.83**	**8.86**	**9.02**	**8.93**	**9.49**
0.023	0.023	1.41	1.31	1.39	0.057
-	-	-	-	-	0.068
0.85	0.85	0.68	0.70	0.35	2.46
12.39	**12.39**	**12.86**	**12.79**	**13.25**	**9.15**
0.734	0.699	0.045	0.05	-	-
0.034	0.03	-	-	-	-
0.027	0.027	0.037	0.04	-	-
45.97	46.03	45.87	45.89	45.84	46.92
99.95	99.99	100.04	100.02	99.99	99.46

Sample preparation

Piz Beverin albite (PB Ab)

First, a polished thin section of a single large cm-sized crystal of Piz Beverin albite, labelled PB0, was prepared in 2020 and analysed by EPMA. After this initial investigation revealed the purity of the Piz Beverin albite, two of the largest sample pieces (> 5 cm) were selected and labelled PB1 and PB2. A third similar piece labelled PB3 was given to the Focused Interest Group on MicroAnalytical Standards (FIGMAS; https://figmas.org; Bullock *et al.* 2021) to Dr. Will Nachlas (U. Wisconsin at Madison; 2020–2022 FIGMAS leader). All samples stem from the same outcrop and are expected to reach the same homogeneity level, but they have been evaluated individually to screen for potential sample-to-sample variation. All results presented here were obtained in samples PB0, PB1 or PB2 (Figure 2a, b).

Assessment of the homogeneity level at the hand-sample scale was performed by cutting through the middle of the largest cm-sized crystal found in each sample, PB1 and PB2. Both cut parts were further broken in two pieces to fit in

CH Masügg PB albite
Hoch Büel Grosswald Bärenbüel
Mittelberg
Sattel
Zwölfihorn
Einshorn
crest
Piz Beverin 500 m

Moraine Nolla schist Carnusa fm. Tomül flysch
Tomül nappe

https://map.geo.admin.ch
© swisstopo.ch

Figure 1. Location of the Piz Beverin albite in canton Graubünden (Switzerland). Geological background map from https://map.geo.admin.ch © swisstopo. See also Wyss and Wiederkehr (2017).

a 1-inch epoxy mould, and were labelled PB1a + PB2a (big, mineral base) and PB1b + PB2b (small, top part, Figure 2c, d). The samples were polished and analysed by SEM for BSE and CL imaging and qualitative ED analysis, then by EPMA for quantitative analyses, and finally by LA-ICP-MS.

Next, two large portions of the PB1 and of PB2 samples were individually crushed and sieved to obtain small grains suitable for microanalysis, ideally in the range > 0.5 to 2 mm. A first attempt at crushing a small piece of PB1 was done by hammer and then by use of a press. Both approaches resulted in overproduction of fine dust. The use of a high-voltage rock fragmentation system "SelFrag" was more efficient at producing coarser grains, less powder, and at liberating minor impurities and inclusions (e.g., Sperner et al. 2014). The resulting grain splits were then sieved to obtain crystal fractions at > 2, 1–2, 0.5–1.0, 0.25–0.50 and < 0.25 mm in PB1 and in PB2 (e.g., Figure 2e–g). Magnetic separation was used to remove some impurities stemming mostly from the host rock, yet careful handpicking was still necessary to remove grains with visible impurities. Nonetheless, an overall mineral separate purity well above 99.5% is estimated. Two sets of "translucent to clear" and "milky" albite grains (four to five grains each) were randomly picked from the two final mineral separates of PB1 (fraction 0.5 to 1.0 mm) and of PB2 (fraction 1 to 2 mm). These grains were mounted in epoxy, polished and analysed by EPMA to ascertain homogeneity after mineral separation (Figure 2e, f).

Several batches of about ten grains of PB1 or PB2 (mineral fractions 0.5–1 or 1–2 mm) were given to the

external co-authors of this paper for evaluation by EPMA. Except for data from ETH Zürich (lab F), all data from the other eight laboratories participating in this study have been anonymised and are referred to herein as labs A to I.

K-feldspar minerals

One large grain (~ 0.5 to 2 cm) of each potential K-feldspar μRM was mounted in epoxy and polished for homogeneity tests by EPMA. For sample S231, two distinct cm-sized grains were mounted and analysed in two separate EPMA sessions and one LA-ICP-MS session. As the quantity of the original K-feldspar samples investigated is currently limited, none of the K-feldspar minerals could be analysed by XRF.

Analytical methods

All polished samples were first observed on a JEOL-6390LA SEM at ETH Zürich to collect backscattered electron (BSE) and cathodoluminescence (CL) images. Analytical conditions were 15 keV and ~ 2 to 3 nA beam current. Rare micro-impurities detected by BSE were qualitatively identified using a 30 mm^2 Thermo Ultradry SDD-ED X-ray detector at a working distance of ~ 10 mm. Preliminary standard-based quantitative ED analyses were also performed on each feldspar sample (not presented here).

Qualitative WD spectrometer scans, quantitative analyses and quantitative element maps of major and minor elements were first performed on a JEOL JXA-8230 EPMA at ETH Zürich. Qualitative WD scans were used to identify all elements present above ~ 200 μg g^{-1} and thus to assess the list of elements to be determined by EPMA (see online supporting information Table S1 for WD scan on LDE1, TAP, TAP-H, PET-L and LiF-H monochromators). The programs "Probe for EPMA", "ProbeImage" and "CalcImage" from ProbeSoftware, inc. were used to acquire and quantify point analyses and element maps (Donovan et al. 2021) on the EPMA at ETH Zürich. Most analyses were performed at 15 keV. Additional analyses on mineral separates of PB1 and PB2 were acquired at 10 keV, and focussed solely on Si, Al, Ca, Na and K. The beam current was set to 20 nA with a beam defocused to 5 or 10 μm to mitigate beam damage and alkali migration.

Extensive stability tests were performed by monitoring the change of Si Kα, Al Kα and Na Kα count rate over time using variable beam current and beam size, from 5 to 50 nA and from ~ 0.5 μm (focused) to ~ 20 μm beam size (see
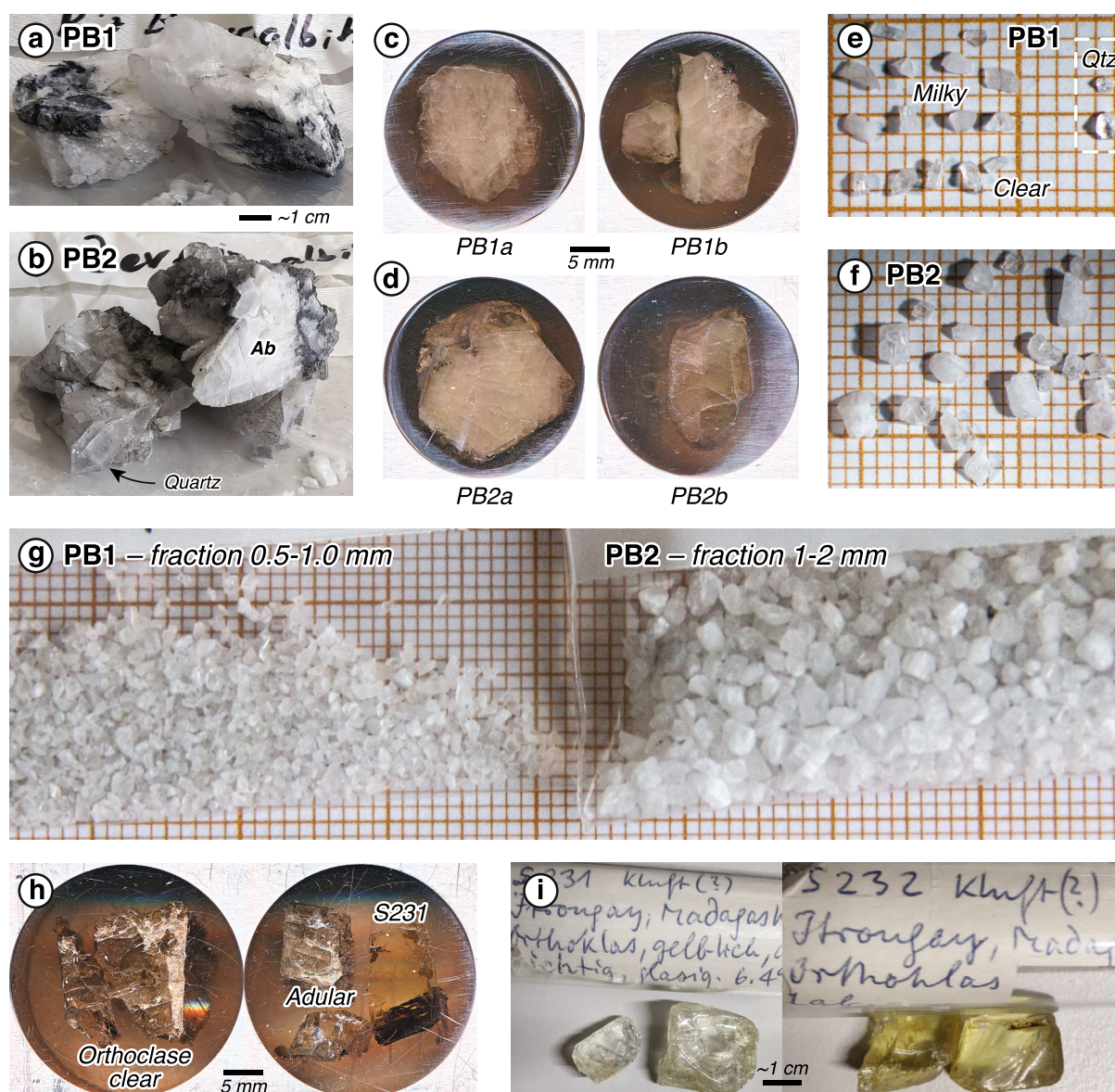
Figure 2. (a, b) Photographs of the albite hand specimens PB1 and PB2. (c, d) Polished round mount of PB1 for homogeneity testing. (e, f, g) Example of mineral separation of PB1 (fraction 0.5–1.0 mm) and PB2 (fraction 1–2 mm) after hand-picking. Some quartz visible on the right side of (e) is rarely found among the albite grains. (h) Scan of two polished mounts of clear K-feldspar "ETH Orthoclase" and of "ETH Adular" and yellow Madagascar sanidine S231. A separate mount (not shown here) was prepared for sample S231 (2nd grain), S232 and Peretti Kfsp. (i) Photos of the gem-quality Madagascar sanidine S231 (left, light yellow) and Fe-richer S232 (right, darker yellow).

Figure 3 and online supporting information Figure S1). At 15 keV, PB albite remains stable up to an electron dose of ~ 5000 nC (= nA s) at 5 μm (= 250 s analysis time at 20 nA) or ~ 10000 nC at 10 μm beam size (= 500 s at 20 nA). A focused beam (≤ 1 μm) should be avoided as the beam damage effect will become almost immediate (maximum dose ~ 700 nC on a W-gun at 15 keV, i.e., less than 35 s at 20 nA), and this effect is expected to be worse with a smaller focused electron beam such as on instruments equipped with a field emission electron source.

The beam damage effect at any voltage, beam size and beam current conditions is better evaluated when considering the total beam power density (e.g., Gunn et al. 1986), or better, the total beam energy density in joules per unit area that is the product of acceleration voltage (keV), electron
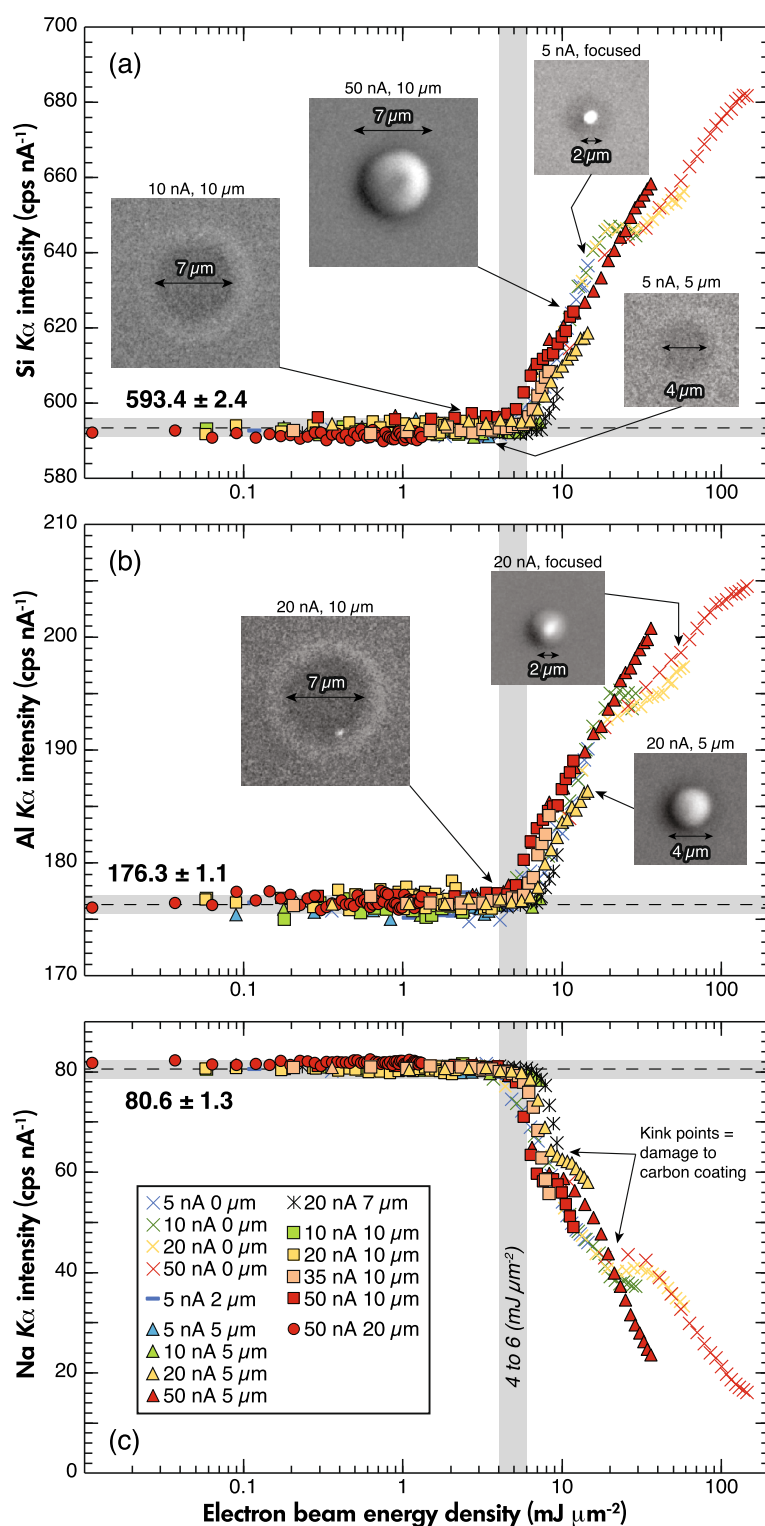
Figure 3. Electron beam energy density plots for Piz Beverin albite obtained at 15 keV for various beam currents and beam diameters for (a) Si $K\alpha$, (b) Al $K\alpha$ and (c) Na $K\alpha$. The effective electron beam diameter was evaluated from SE imaging revealing carbon contamination and potential beam damage left after the 10-minute stability test, as shown in (a) and (b) for various beam conditions. Electron beam energy density is expressed in millijoules per square micrometre (= keV nA s μm^{-2}). Horizontal grey bands represent the mean count rates and uncertainties with no beam damage. Vertical grey bands indicate the approximate threshold before significant beam damage.

Table 2.
Electron probe microanalysis set-ups at ETH Zürich (JEOL JXA-8230, W-gun)

(a) Complete set-up at 15 or 10 keV analysis

SP	El. Line	Crystal	Peak (s)	Bkg (s)	Bkg +	Bkg −	Bkg type	Primary reference material
1	Si Kα	TAP	30	0 or 30	3.5	-7	MAN or 2-pts	H021 - Albite (Tiburon, CA, USA)
1	Al Kα	TAP	30	0 or 30	3.5	-2.5	MAN or 2-pts	H103 - Anorthite (U. Wien, Austria)
2	K Kα	PETJ	30	0 or 30	3	-3	MAN or 2-pts	MCL - Microcline (Smithsonian)
2	Ti Kα	PETJ	30	0	-	-	MAN	D015 - Rutile (synthetic)
3	Ca Kα	PET-L	30	0 or 30	4	-3	MAN or 2-pts	H103 - Anorthite (U. Wien, Austria)
3	Cr Kα	PET-L	30	0	-	-	MAN	D028 - Chromite (Stillwater, MT, USA)
4	Fe Kα	LIF-H	30	0	-	-	MAN	H116 - Fayalite (synthetic)
4	Mn Kα	LIF-H	30	0	-	-	MAN	D023 - Pyrolusite (synthetic)
5	Na Kα	TAP-H	30	0 or 30	5.5	-5	MAN or 2-pts	H021 - Albite (Tiburon, CA, USA)
5	Mg Kα	TAP-H	30	0	-	-	MAN	H083 - Forsterite (synthetic)

(b) Simple set-up (15 keV only)

SP	El. Line	Crystal	Peak (s)	Bkg (s)	Bkg +	Bkg −	Bkg type	Primary reference material
1	Si Kα	TAP	30	0	-	-	MAN	H021 - Albite (Tiburon, CA, USA)
2	Al Kα	TAP	30	0	-	-	MAN	H103 - Anorthite (U. Wien, Austria)
3	Ca Kα	PET-L	30	0	-	-	MAN	H103 - Anorthite (U. Wien, Austria)
4	K Kα	PET-H	30	0	-	-	MAN	MCL - Microcline (Smithsonian)
5	Na Kα	TAP-H	30	0	-	-	MAN	H021 - Albite (Tiburon, CA, USA)

(c) Set-up for K-feldspar (15 keV)

SP	El. Line	Crystal	Peak (s)	Bkg (s)	Bkg +	Bkg −	Bkg type	Primary reference material
1	Si Kα	TAP	15	0	-	-	MAN	H021 - Albite (Tiburon, CA, USA)
1	Al Kα	TAP	15	0	-	-	MAN	H103 - Anorthite (U. Wien, Austria)
2	K Kα	PET-H	40	0	-	-	MAN	MCL - Microcline (Smithsonian)
3	Ba Kα	PET-L	40	0	-	-	MAN	F002 - Barite (R. Oberhänsli, Switzerland)
4	Fe Kα	LIF-H	40	0	-	-	MAN	H116 - Fayalite (synthetic)
5	Na Kα	TAP-H	40	0	-	-	MAN	H021 - Albite (Tiburon, CA, USA)

Most analyses of PB albite were obtained using the simple five-element set-up.
A summary of the EPMA analytical set-ups of external laboratories can be found in Table S2.
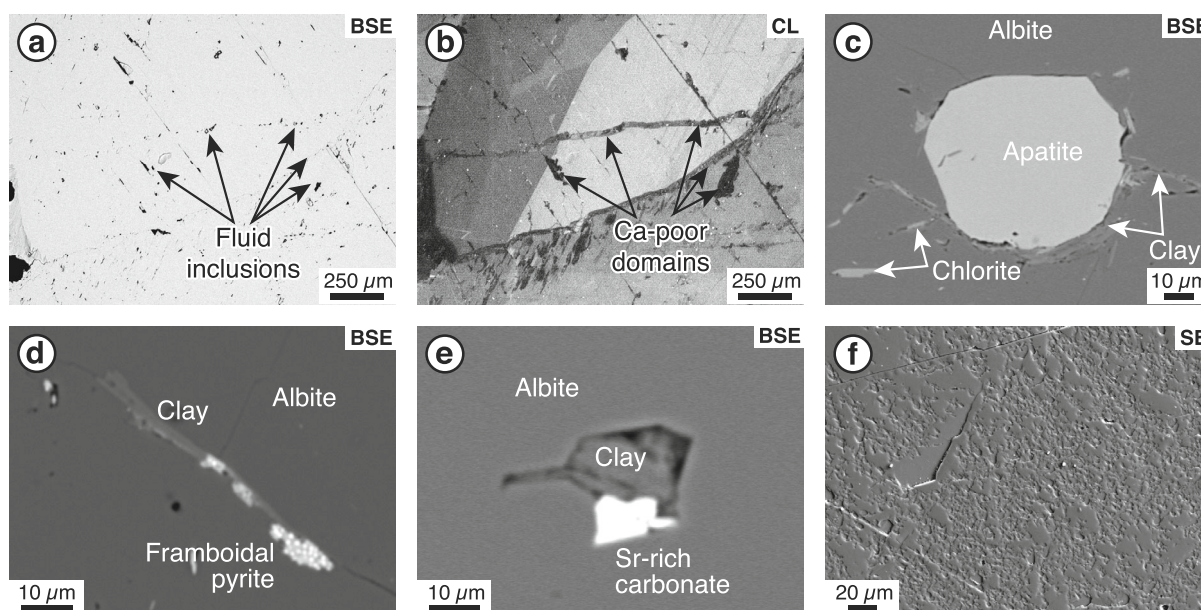
Figure 4. (a) BSE and (b) CL images of the same area in a large crystal of PB1. The patchy CL texture can be seen throughout the grain. The lowest CL signal area matches low Ca-content. See text for details. (c) A rare and exceptionally large apatite inclusion in PB1, accompanied by small flakes of clay and chlorite. (d, e) Other "common" yet rare micro-inclusions of clay, carbonate (calcite and Ca ± Sr-rich carbonate) and framboidal pyrite. (f) Difficult to polish surface of a PB albite single grain mounted parallel to its main crystallographic plane, most likely resulting from a high density of fluid inclusions on the polished plane.

Table 3.
EPMA mean measurement results for the Piz Beverin albite in % *m/m*

(a) Round robin evaluation and primary data in PB0 (lab F)

Lab ID	A	B	C	D	E	F (ETHZ)	G	H	I
Comment	Multiple grains (> 5)					PB0 grid	2 grains	10 grains	3 grains
# points	80	278	383	310	87	121	44	515	130
Si	32.3(3)	32.0(8)	31.89(23)	32.0(7)	31.8(3)	32.17(24)	32.13(25)	32.19(18)	32.03(26)
Al	10.1(3)	10.26(19)	10.49(10)	10.44(19)	10.48(18)	10.35(10)	10.38(13)	10.32(25)	10.48(6)
Ca	0.05(4)	0.06(3)	0.05(4)	0.06(5)	0.04(5)	0.05(4)	0.04(2)	0.05(3)	0.059(22)
Na	8.66(20)	8.62(24)	8.79(10)	8.70(29)	8.65(16)	8.66(8)	8.56(12)	8.73(18)	8.81(14)
K	< 0.015	< 0.016	0.016(8)	0.018(8)	0.011(8)	0.019(7)	0.014(13)	0.011(6)	0.014(8)
Sr	< 0.13	0.10(16)	n.a.	n.a.	0.042(26)	0.022(20)	n.a.	n.a.	n.a.
O*	48.8(5)	48.6(9)	48.8(3)	48.8(8)	48.6(4)	48.9(3)	48.8(3)	48.9(3)	48.9(3)
Total	99.83	99.61	100.01	100.08	99.59	100.18	99.95	100.21	100.30
QF Si	1.22	3.16	0.89	2.66	1.24	0.96	1.00	0.69	1.04
QF Al	2.88	2.02	1.01	1.81	1.92	1.01	1.32	2.61	0.59
QF Na	2.43	2.86	1.13	3.43	1.94	0.97	1.42	2.12	1.77

(b) Additional data from ETH Zürich

Sample	PB 1a	PB1b big	PB1b sm.	PB2a	PB2b	PB1a	PB1a
Comment	Line	Line	Line	Line	Line	#1 w/bkg	#3 w/bkg
# points	55	46	20	55	56	45	30
Si	32.41(20)	32.64(17)	32.66(15)	32.36(13)	32.4(3)	32.5(3)	32.2(4)
Al	10.44(9)	10.37(8)	10.37(7)	10.48(7)	10.40(8)	10.38(11)	10.38(11)
Ca	0.06(3)	0.06(3)	0.047(19)	0.05(3)	0.034(17)	0.05(3)	0.06(3)
Na	8.64(10)	8.68(7)	8.70(9)	8.71(11)	8.71(6)	8.73(9)	8.68(10)
K	0.016(12)	0.014(5)	0.013(5)	0.013(7)	0.014(5)	0.015(8)	0.016(12)
Sr	n.a.	n.a.	n.a.	n.a.	n.a.	n.a.	n.a.
O*	49.2(3)	49.46(22)	49.49(18)	49.24(16)	49.3(3)	49.3(4)	49.0(5)
Total	100.81	101.23	101.28	100.85	100.86	100.91	100.41
QF Si	0.79	0.66	0.58	0.53	1.01	1.27	1.41
QF Al	0.88	0.83	0.67	0.70	0.83	1.09	1.10
QF Na	1.21	0.90	1.10	1.22	0.71	1.09	1.20

All data are given with 2*s* uncertainty in parentheses; the uncertainty was calculated from the standard deviation of repeated analysis. Standard errors can be calculated using the number of analysed points given in the heading of each column. Oxygen determined by stoichiometry assuming Si^{4+}, Al^{3+}, Ca^{2+}, Sr^{2+}, Na^+ and K^+.

QF = quality factor (Potts and Webb 2022).

* Oxygen calculated by stoichiometry.

beam current (nA) and time (s), all normalised to the affected area (μm^2). The effective beam diameter was evaluated by observing the weak to strong damage left on the 20 nm carbon coating after each 10-minute analysis (Figure 3a, b). At the considered beam aperture #2, the effective beam diameter above 2 µm is approximately 10 to 20% smaller than the value indicated by the software (which is calibrated for beam aperture #1), as determined by observing the damaged area using a high magnification SE imaging and measuring the carbon contamination or damaged spot. Carbon-contamination occurs around each analysis spot, with the formation of a C-ring around the point of impact of the electron beam (e.g., Buse and Stern 2015). When beam damage is pronounced, a clear bright spot in the middle is visible in addition to the carbon-ring and matches with the appearance of a kink visible on all elements in the Figure 3 after 9 to 11 mJ μm^{-2}. We hypothesise that either (1) the

carbon coating is mostly gone (charging) or (2) the matrix has densified. For the calculation of the total beam energy density, the effective beam diameter of a "focused" beam size was set to 2 µm to better represent the activation volume (~ 2 µm in diameter according to a Casino Monte Carlo simulation; Drouin *et al.* 2007) which, with a low mean atomic number target, is much larger than the true electron beam size (estimated at 0.7 to 0.5 µm with a W-filament at 15 keV). Overall, the beam damage was significant at an electron beam energy density of 4 to 6 mJ μm^{-2} (Figure 3), and correctable with a TDI correction up to 9 mJ μm^{-2} when a 20 nm C-coating was applied, although this possibly depends on the quality of the conductive coating applied and could be higher with different coating materials. A kink point is visible in Figure 3 around 8 to 30 mJ μm^{-2}, beyond the initial beam damage effect. This point is probably related to the irreversible damage of the conductive carbon coating

GEOSTANDARDS and GEOANALYTICAL RESEARCH

Table 4.
LA-ICP-MS measurement results from the Piz Beverin Albite Pb1a, including bright and dark CL images

El.	Mass	Min	Max	% < DL	Line 1 50 pts	Line 2 50 pts	Bright CL 10 pts	Dark CL 10 pts
Si % m/m	29	30.44	33.00	0%	31.6(1.0)	31.5(9)	31.3(1.1)	31.2(5)
Al (IS)	-	-	-	-	10.39	10.39	10.39	10.39
Na % m/m	23	8.37	9.39	0%	8.80(37)	8.74(31)	8.70(22)	8.60(16)
Values below in $\mu g\ g^{-1}$								
Ca43*	43	266	2295	0%	1375(330)	1590(650)	1260(190)	1430(630)
Ca42*	42	17	706	0%	330(470)	-	-	-
Sr	88	65.2	477.1	0%	300(160)	340(130)	270(30)	280(140)
K	39	43.0	147.1	0%	95(47)	100(38)	96(23)	84(24)
Ba	137	0.5	7.8	0%	1.4(1.0)	1.6(2.2)	0.91(20)	0.8(5)
Be	9	0.038	0.718	0%	0.29(27)	0.30(21)	0.39(21)	0.25(11)
Pb	208	0.016	0.791	0%	0.5(4)	0.5(3)	0.47(9)	0.45(20)
Values below are indicative (near $\mu g\ g^{-1}$ and close to or below DL)								
Mg	24	< 0.4	6.9	36.7%	1.5(2.5)	1.2(1.7)	2.0(2.0)	0.7(4)
Sc	45	< 0.14	0.51	15.8%	0.31(13)	0.26(14)	0.27(13)	0.23(12)
Zn	66	< 0.14	51.72	45.0%	2(9)	6(24)	0.3(3)	0.42(65)
Eu	151	< 0.0005	0.0123	4.2%	0.0049(50)	0.006(6)	0.0053(23)	0.0039(21)

% < DL = percentage of analysis points below detection limit.
* Mass Ca43 shows interference from AlO^+ ion. Mass Ca42 yielded more accurate results.

Table 5.
XRF measurement results for samples PB1 and PB2 of the Pz Beverin albite (units in % m/m, except Sr and Sc in $\mu g\ g^{-1}$)

	PB 1	PB 2a	Unc. (2s)
Si	31.80	32.16	0.14
Ti	< 0.008	< 0.008	-
Al	10.31	9.94	0.06
Fe^{3+}	< 0.01	< 0.01	-
Mn	< 0.0012	< 0.0009	-
Mg	< 0.0025	< 0.002	-
Ca	0.047	0.034	0.0330
Na	8.532	8.222	0.063
K	0.015	0.014	0.018
P	0.002	0.002	0.003
O	48.40	48.36	-
LOI	0.32	0.21	-
Total	99.44	98.95	-
Sr ($\mu g\ g^{-1}$)	344.5	336.7	4.1
Sc ($\mu g\ g^{-1}$)	5.7	8.9	3.8

LOI = Loss on ignition.

the same spectrometer, notably for the preliminary homogeneity tests in PB0 that included Fe, Mg, Mn, Sr, Ti and Cr. Barium was added to each analysis of K-feldspar. A single analysis lasted between 30 and 90 s, with a shorter acquisition time for the quick five-element analyses with Mean Atomic Number (MAN) background correction (Donovan and Tingle 1996, Donovan et al. 2016). In all cases, no diffusion or beam damage was observed after the quantitative analysis, besides minor damage to the carbon coating. To ensure accuracy of the MAN-background approach for minor elements (e.g., Ca and K in PB albite), a few measurements were done with a classical two-point background acquisition and a linear interpolation. Natural and synthetic internal μRM were used for the quantification (Table 2). Additional simple synthetic and natural oxide μRM including SiO_2, Al_2O_3, MgO, Fe_2O_3 and TiO_2 were measured to help constrain the MAN background correction. Each primary μRM was measured before and after the analysis, and a correction on possible drift in standard intensities was applied. Quantification was done using the Armstrong φ(ρz) matrix correction (Armstrong 1988) using the FFAST mass absorption coefficient table (Chantler et al. 2005). Samples PB1, S231 and the two clear K-feldspars were also quantitatively mapped for their major and minor elements (Si Kα, Al Kα, Na Kα, K Kα and Ca Kα or Ba Lα) using the mapping quantification routine described in Donovan et al. (2021) and using a MAN background correction.

layer that induces surface charging, potentially causing a back-diffusion of alkali ions (hence a brief apparent stability in count rates), combined with a local change in the mean atomic number due to the volatilisation or diffusion of some elements (e.g., Na in the case of albite).

For accurate quantitative determination, all major elements were measured first (Si, Al, Ca, Na and K), except for some analyses where Al was determined ~ 30 s after Si on

Two samples from Piz Beverin albite (PB1 and PB2) and one yellow Madagascar K-feldspar (S231) were further

GEOSTANDARDS and GEOANALYTICAL RESEARCH

Table 6.
Summary of EPMA, LA-ICP-MS and XRF analyses of the Piz Beverin albite in % *m/m*, and atom per formula recalculation based on eight oxygen atoms. The recommended values to be used for this micro reference material are listed in the last column

| Element | Raw data | | | Normalised to 100% | | | Recommended | |
	EPMA*	LA-ICP-MS	XRF (PB1)	EPMA	LA-ICP-MS	XRF (PB1)	value (% m/m)	Std error
Si	32.05(60)	31.6(1.0)	31.80(14)	32.05	31.9	32.0	**32.08**	**0.10**
Al	10.38(30)	*10.39 (IS)*	10.31(6)	10.38	*10.49*	10.37	**10.43**	**0.09**
Sr	~ *0.033***	0.032(13)	0.0344(4)	~ *0.03***	0.032	0.035	*0.032*	*0.013*
Ca	0.05(4)	0.03(5)	0.047(33)	0.05	0.033	0.047	*0.052*	*0.005*
Na	8.71(24)	8.7(9)	8.53(6)	8.71	8.83	8.58	**8.69**	**0.05**
K	0.014(7)	0.010(4)	0.015(18)	0.014	0.0097	0.015	*0.015*	*0.002*
O (calc.)	*48.8(7)*	*48.3*	*48.4*	*48.8*	*48.7*	*48.7*	*48.88*	
TOTAL	**100.04**	**99.1**	**99.5**	**100.0**	**100.0**	**100.0**	100.18	
Si	2.993	*2.980*	2.994	2.993	*2.980*	2.994	2.9910	
Al	1.009	*1.021*	1.011	1.008	*1.021*	1.010	1.0122	
Sr	0.0010	0.0010	0.0011	0.0009	0.0010	0.0010	0.0010	
Ca	0.0035	0.0022	0.0031	0.0033	0.0022	0.0031	0.0034	
Na	0.994	*1.009*	0.981	0.994	*1.009*	0.981	0.9897	
K	0.0010	0.0007	0.0010	0.0010	0.0007	0.0010	0.0010	
Total cation	**5.0003**	5.014	4.992	**5.000**	5.014	4.992	4.9982	
O	*8.0000*	*8.0000*	*8.0000*	*8.0000*	*8.0000*	*8.0000*	*8.0000*	
Ca+Na+K+Sr	0.9990	1.0130	0.9866	0.9989	1.0129	0.9866	0.9951	
% X$_{Ab}$	99.46%	99.62%	99.48%	99.49%	99.62%	99.48%	**99.47%**	**0.20%**

IS = internal standard.
X$_{Ab}$ = Na / (Ca + Na + K + Sr).
* Mean of all EPMA measurement results from all nine laboratories A to I.
** Only two EPMA labs reported significant amount of Sr data above detection limit: lab E at 0.042(26) and lab F at 0.022(20). Both labs included a correction for the interference of satellite Si *K*-lines over Sr *L*α.

investigated by LA-ICP-MS at ETH Zürich for trace element content and additional homogeneity tests. The laser ablation system used was a Resolution S-155 (193 nm wavelength) laser with a Laurin Technic dual volume S-155 cell (~ 1 cm^3 effective volume); repetition rate was set at 5 Hz, spot diameter at 29 μm, and energy density at 3.5 J cm^{-2}. Background acquisition and ablation duration were both set to 30 s. The ablation aerosol was mixed in the ablation cell with carrier gas consisting of helium (~ 0.5 l min^{-1}) and make-up gas consisting of argon (~ 1 l min^{-1}) and nitrogen (2 ml min^{-1}). The ablated aerosol was then homogenised by flushing through an in-house built squid device before introduction into the ICP-MS. Analyses were performed on a Thermo Element XR sector field single-collector ICP-MS. Before each measurement session the instrument was optimised on NIST SRM 612 glass to achieve a detection efficiency in the range of 2% (on Pb, Th, U) while keeping oxide production low (^{248}ThO$^+$/^{232}Th$^+$ ≤ 0.25%) and a U/Th ratio of ~ 1. Aluminium was selected as the internal standard element using the value obtained on the initial EPMA data in albite PB0 or in K-feldspar S231 (1st grain). NIST SRM 612 was used as a RM with identical ablation parameters. Although LA-ICP-MS data are less accurate for major element determination compared with EPMA,

the measurement results remain very precise and can therefore be used to assess the homogeneity level of major elements, along with the precision and accurate variability of minor to trace element contents. The initial analyses of PB1 looked for mass ^{43}Ca, which was found to significantly interfere with the ^{27}Al^{16}O$^+$ ion. A few additional and more accurate measurements were performed using mass ^{42}Ca.

Two multi-grain sets of ~ 2 g each taken from the PB1 or PB2 mineral separates were prepared for bulk XRF analysis. The loss on ignition at 1050 °C was determined from approximately 1.2 g of sample powder and then mixed with lithium tetraborate(66%)-metaborate(34%) at a ratio of 1:7. The mixtures were melted into glasses using the Eagon 2 from Malvern-Panalytical and analysed by XRF using a Malvern-Panalytical Axios at ETH Zürich.

Analytical uncertainties are all listed at the 2*s* level (95.5% confidence). Uncertainties on individual EPMA and XRF measurements stem from the counting statistics on RM and unknowns. The uncertainties on multiple EPMA and LA-ICP-MS analyses are based on the standard deviation of all repetitions, and the number of points averaged is indicated
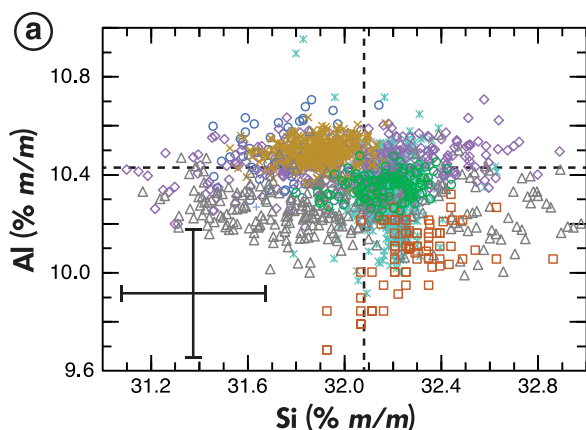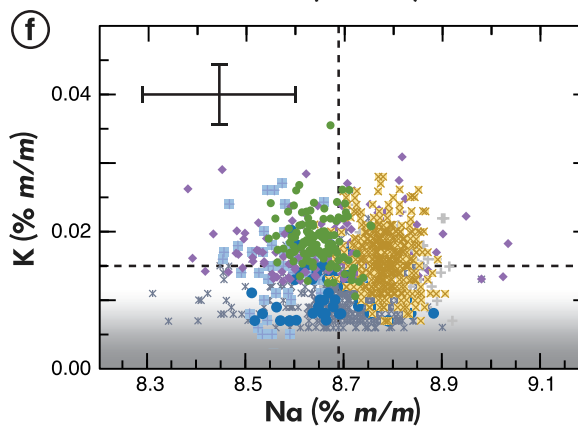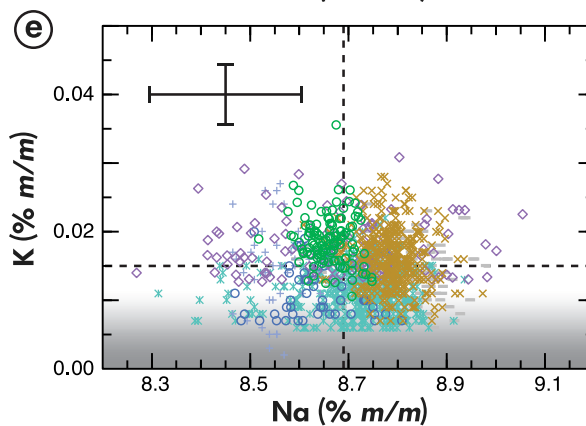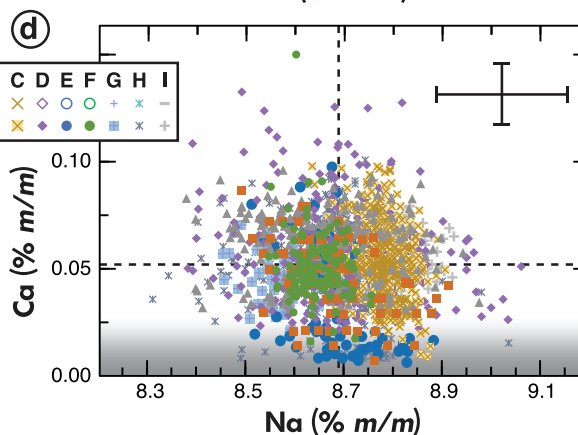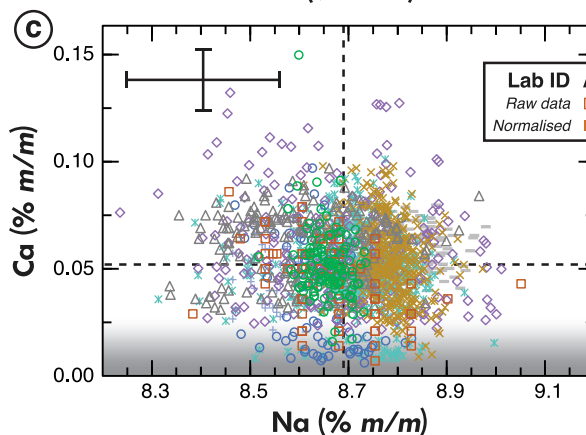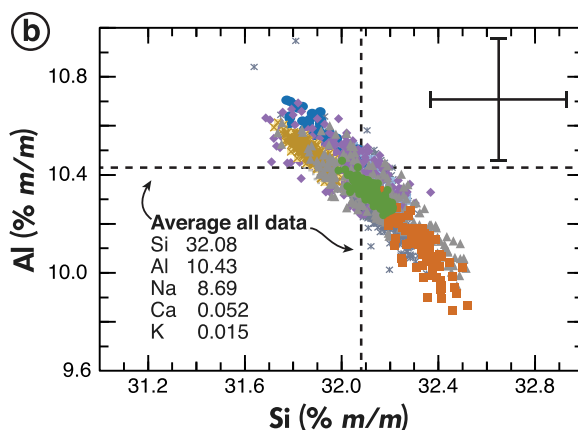
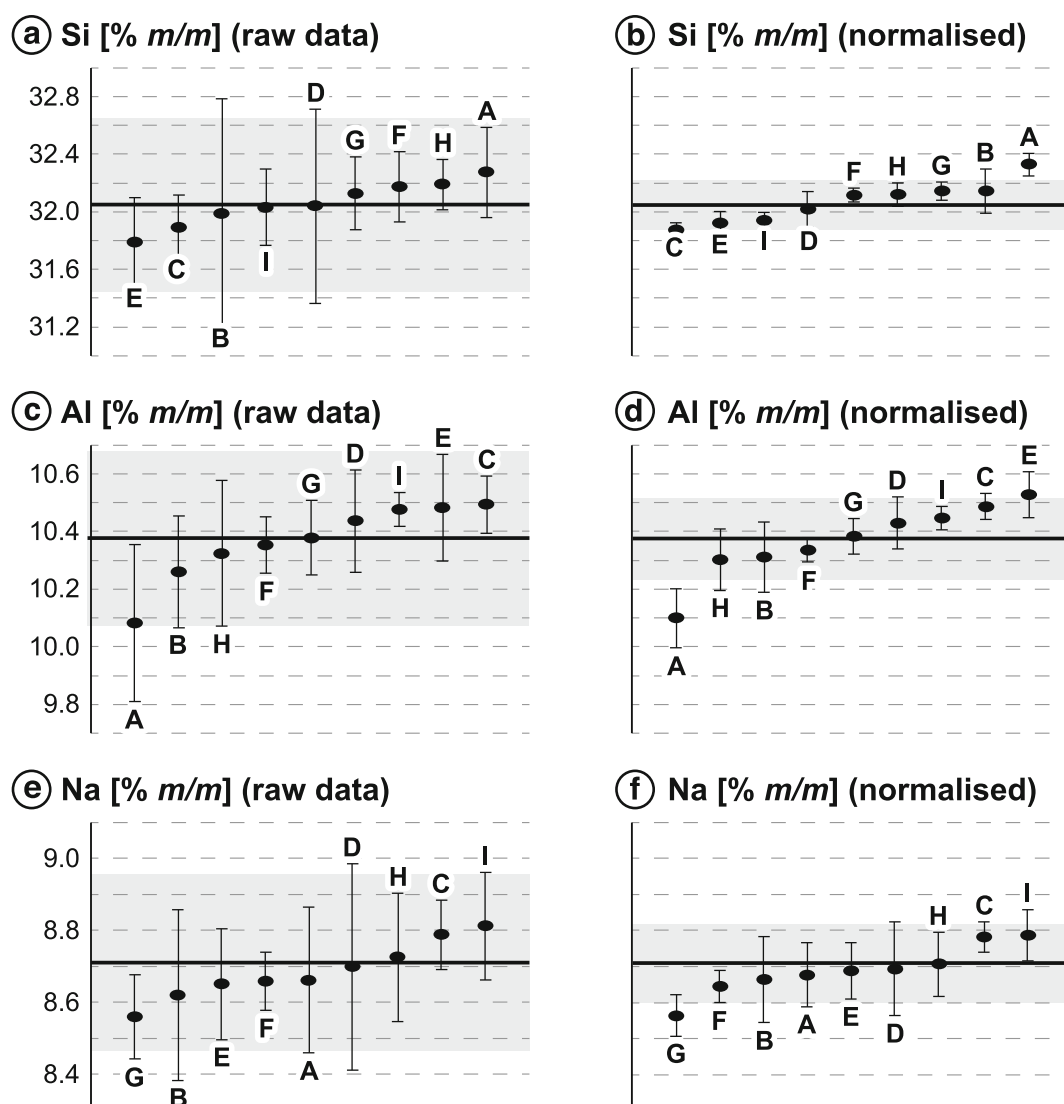**Figure 5.** Quantitative EPMA measurements for PB1 and PB2 from nine independent EPMA laboratories (raw data and normalised to 100% total). (a, b) Si *vs.* Al % *m/m*. (c, d) Na *vs.* Ca % *m/m*. (e, f) Na *vs.* K % *m/m*. Grey shaded areas represent detection limits from the different laboratories and the range bars represent the mean uncertainty on individual point analyses (both of which vary slightly depending on the analytical conditions of each lab; see exact standard deviation of each lab in Table 3). All data are available in Tables S3 (ETH Zürich data) and S4 (external laboratories).

in the headings of each table. Detection limits are expressed at the 3*s* level (99.7% confidence). A summary of EPMA analytical conditions for each participating external laboratory is summarised in Table S2.

For an indirect structural characterisation, a Raman spectrum was acquired with a DILOR Labram Raman spectrometer at 300 mm focal length and an 1800 g mm⁻¹ grating in unpolarised backscattering with a 532 nm laser.

© 2023 The Authors. *Geostandards and Geoanalytical Research* published by John Wiley & Sons Ltd on behalf of International Association of Geoanalysts.

Figure 6. Results of round robin evaluation with mean and 2s standard deviation in % *m/m* of each laboratory A to I, ordered by increasing content of (a, b) Si, (c, d) Al and (e, f) Na. Means and 2s standard deviation of mean (grey band) were calculated using respectively the all raw or normalised data of all labs.

The spectrum was recorded through a 50× objective and was averaged over six individual exposures of 10 s each, with a laser power on sample of about 4 mW.
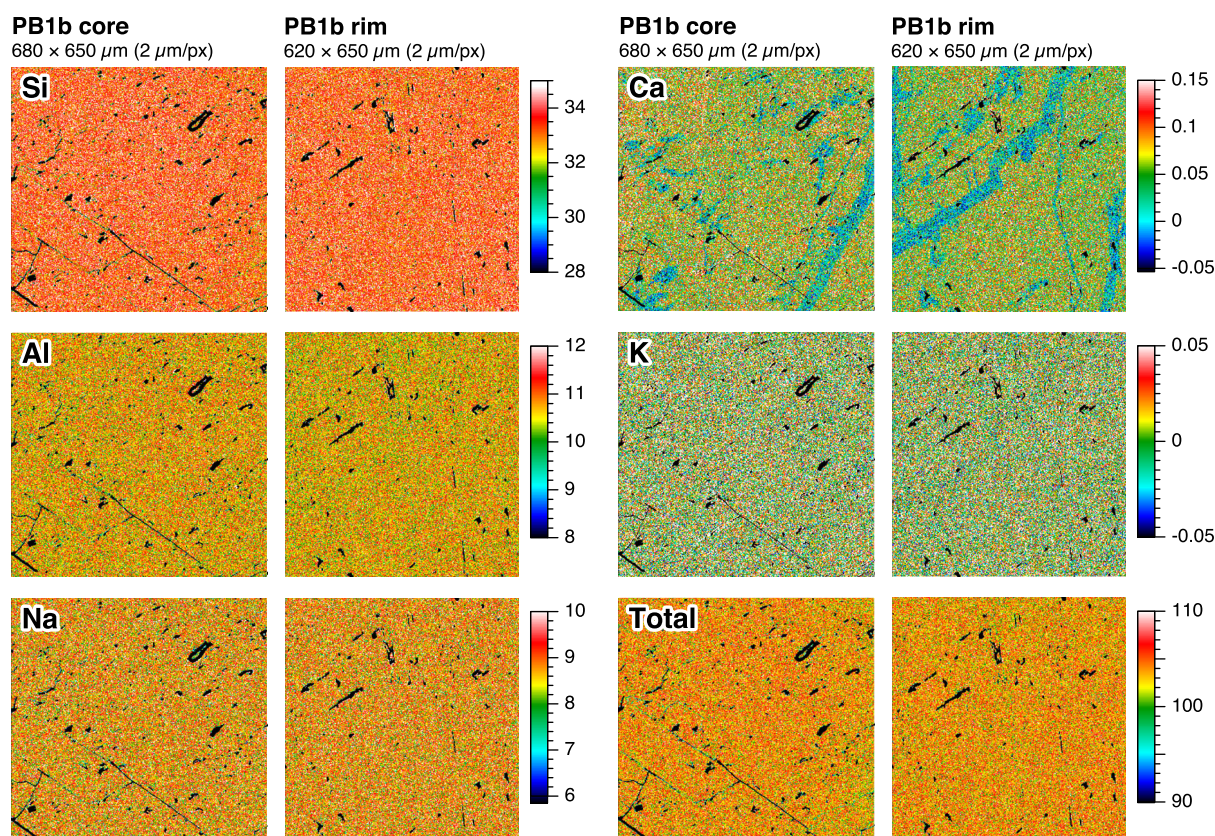
Results and discussion

Piz Beverin albite (PB Ab)

Quality assessment of cm-sized PB1 and PB2 albite single-crystal at the SEM revealed a homogeneous BSE signal, even under high-contrast mode, yet with a significant variation in cathodoluminescence (CL) signal (e.g., Figure 4a, b). Panchromatic CL imaging reveals a patchwork of light- to mid-grey colour domains visible at large scales (> > 100 μm) that are cross-cut by distinct darker vein-like domains of about 50 μm width or less (Figure 4b). BSE imaging revealed extremely rare inclusions and impurities along grain edges and fractures, including calcite (±Sr-rich carbonate), chlorite, muscovite, clay minerals, apatite and framboidal pyrite (Figure 4c–e). Most inclusions are ~ 1–10 μm in size, rarely reaching 50–100 μm (e.g., apatite in Figure 4c). Some albite grains can be locally rich in fluid inclusions, notably along crystallographic planes. Nonetheless, any randomly oriented polished grains should still reveal large fluid-inclusion-free areas (> 50–100 μm) that are suitable for micrometre-scale microanalysis. One external laboratory mentioned an issue with several polished

PB1b core
680 × 650 μm (2 μm/px)

PB1b rim
620 × 650 μm (2 μm/px)

PB1b core
680 × 650 μm (2 μm/px)

PB1b rim
620 × 650 μm (2 μm/px)

Figure 7. Quantitative element map (in % *m/m*) obtained by EPMA in PB1b albite rim and core. Mapping sizes are given atop of each column. Both sets of element maps were acquired at 15 keV, 50 nA, 2 μm beam size, and 50 ms per pixel dwell time, and using the spectrometer set-up listed in Table 2b. Black pixels on the figure correspond to fractures and holes (e.g., fluid inclusions).
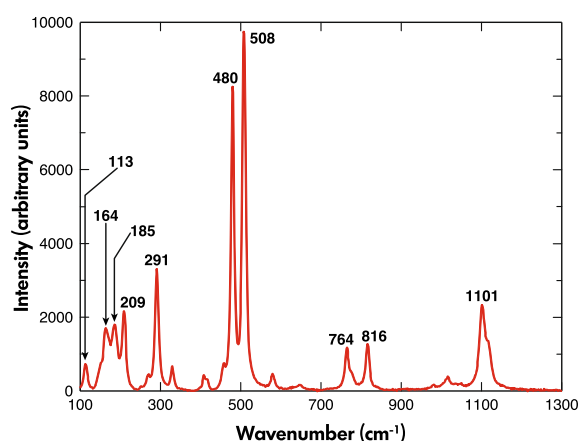
Figure 8. Unpolarised Raman spectrum of PB1 albite. Positions of major peaks are indicated. The measured difference of 28.2 cm^{-1} between 479.6 and 507.8 cm^{-1} points to a low-albite structure. See also RRUFF ID R230008.

grains out of a multiple-grain epoxy mount showing a very rough surface (Figure 4f). These grains were specifically mounted on a cleavage surface and it is possible that a plane with a high-density of fluid inclusions was reached on such grains during the fine-polishing steps, resulting in a difficult to polish surface. Based on this observation, it is recommended to avoid mounting single grains of this PB albite μRM on a cleavage plane. Mounts of macroscopically "clear" versus "milky" grains of this albite both seem to have equal areas of higher density fluid inclusions.

Representative mean EPMA compositions are presented in Table 3, including data from the participating external EPMA laboratories. LA-ICP-MS and XRF data are shown in Tables 4 and 5, respectively. All analyses are summarised in Table 6 and accompanied by a set of recommended values for this μRM. The complete sets of EPMA data are available in Tables S3 (ETH Zürich) and S4 (external labs). EPMA data from all laboratories for Si, Al, Ca, Na and K are plotted in

Table 7.
EPMA measurement results (in % *m/m*) of the five K-feldspar minerals investigated

Sample	Yellow Madagascar sanidine crystals				ETH orthoclase			ETH adular		
	S231 (a)	S231 (b)	S232	Peretti	Mean	*Dark*	*Bright*	Mean	Domain 1	Domain 2
Comment	Grain 1	Grain 2	All pts	All pts	All pts	*Rare*	*Most pts*	All pts	*High-Ba*	*Rim low Ba*
# points	160	130	100	100	85	10	40	87	14	10
Si	30.35(25)	30.18(17)	29.76(28)	30.09(14)	29.5(6)	*30.17(8)*	*29.38(18)*	29.8(3)	*29.75(24)*	*29.91(18)*
Al	9.48(9)	9.56(9)	8.65(10)	8.85(10)	*10.03(10)*	*9.78(5)*	*10.08(7)*	9.98(10)	*9.97(9)*	*9.83(11)*
Fe	0.359(19)	0.362(25)	1.92(5)	1.33(3)	*< 0.010*	*< 0.010*	*< 0.010*	< 0.010	*< 0.010*	*< 0.010*
Ca	< 0.005	n.a.	n.a.	n.a.	< 0.005	*< 0.005*	*< 0.005*	< 0.005	*< 0.005*	*< 0.005*
Na	0.418(15)	0.415(19)	0.312(20)	0.644(19)	0.7(4)	*0.13(5)*	*0.82(3)*	0.7(4)	*0.27(3)*	*0.16(5)*
K	13.32(10)	13.48(11)	13.52(12)	13.04(10)	12.4(1.2)	*13.98(5)*	*12.11(13)*	12.7(6)	*13.38(16)*	*13.77(14)*
Ba	*n.a.*	< 0.013	0.075(16)	0.036(15)	1.5(1.2)	*0.01*	*1.80(15)*	0.8(3)	*1.03*	*0.44*
O*	46.00	45.95	45.31	45.62	45.52	*45.98*	*45.41*	45.77	*45.71*	*45.74*
Total	99.93	99.94	99.55	99.62	99.67	*100.05*	*99.61*	99.79	*100.09*	*99.84*
Quality Factors (k = 0.01; Potts and Webb 2022)										
QF Si	1.06	0.73	1.17	0.60	2.44	*0.69*	*0.78*	1.24	*1.00*	*0.76*
QF Al	0.96	0.96	1.22	1.13	2.16	*1.12*	*0.75*	1.08	*0.94*	*1.16*
QF K	0.87	0.94	0.97	0.84	10.7	*0.74*	*1.19*	5.15	*1.36*	*1.11*
QF Fe	*3.36*	*4.40*	*1.94*	*2.04*	*-*	*-*	*-*	*-*	*-*	*-*
QF Na	*2.39*	*2.98*	*4.04*	*2.08*	*43.1*	*17.1*	*2.7*	*40.7*	*7.5*	*19.2*
QF Ba	*-*	*-*	10.6	18.3	62.3	*90.9*	*7.0*	27.8	*13.6*	*34.3*

* Calculated by stoichiometry.
The three yellow Madagascar sanidine samples S231, S232 and Peretti appear homogeneous. In contrast, a mean and some extreme variations of composition are shown for the two clear crystals of "ETH Orthoclase" and "ETH Adular", which are shown to be inhomogeneous and not suitable as µRMs.

Figure 5. Results from the inter-laboratory evaluation for Si, Al and Na are summarised in Figure 6. Additional EPMA data included in Table S3 are summarised in plots of Si, Al, Ca, Na, K and Sr in Figure S2. To ease the comparison between different measurement sessions and techniques, data are provided both as raw and as normalised to an assumed 100% *m/m* total (Figures 4,5, Table 6, and Tables S3 and S4). Normalising the data to 100% is acceptable in this case, as the analysed elements plus oxygen by stoichiometry represent > 99.9% of the total elements. Data should never be normalised to 100% if an element is clearly missing (e.g., H, Li, B, Be, C).
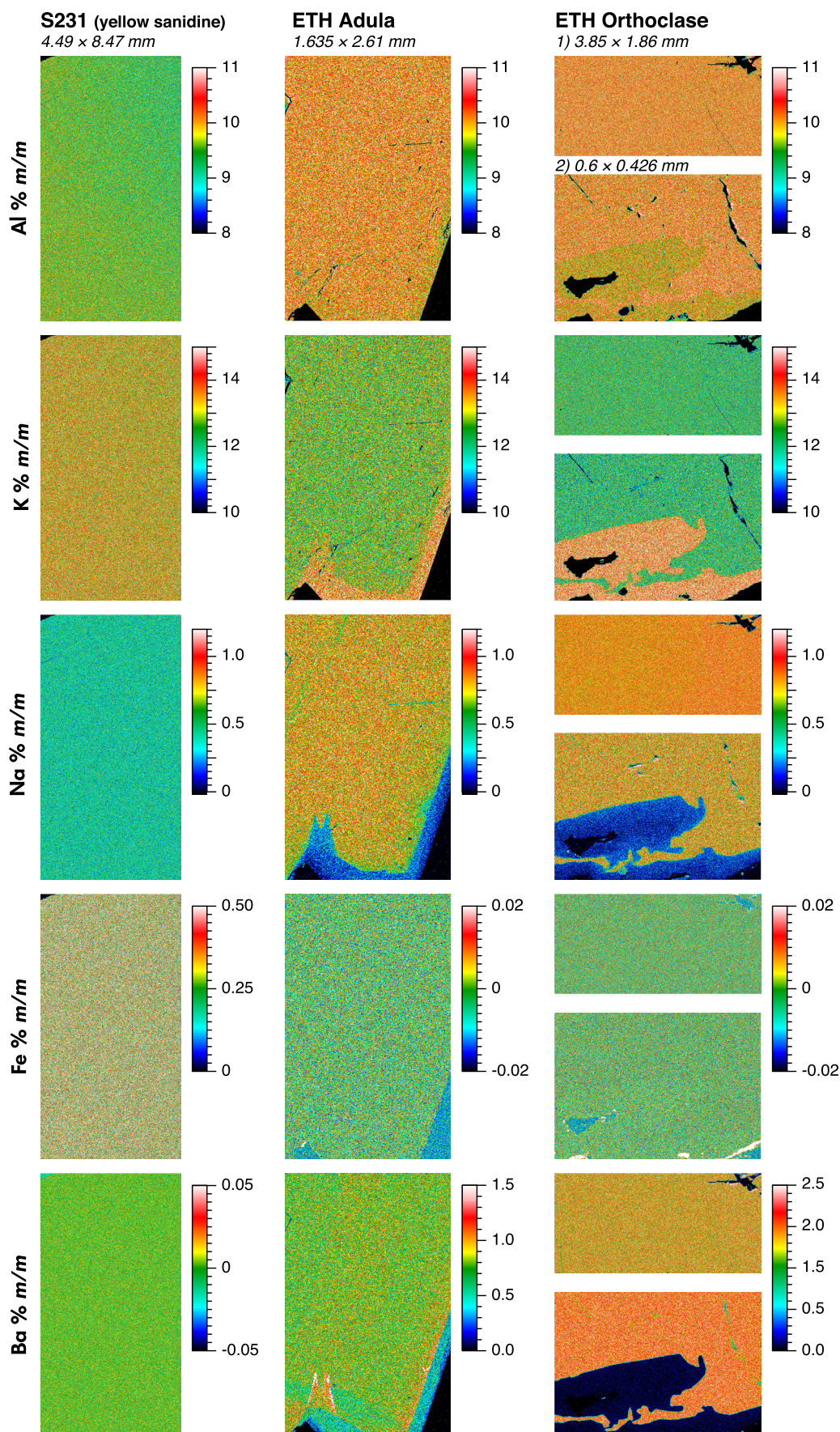
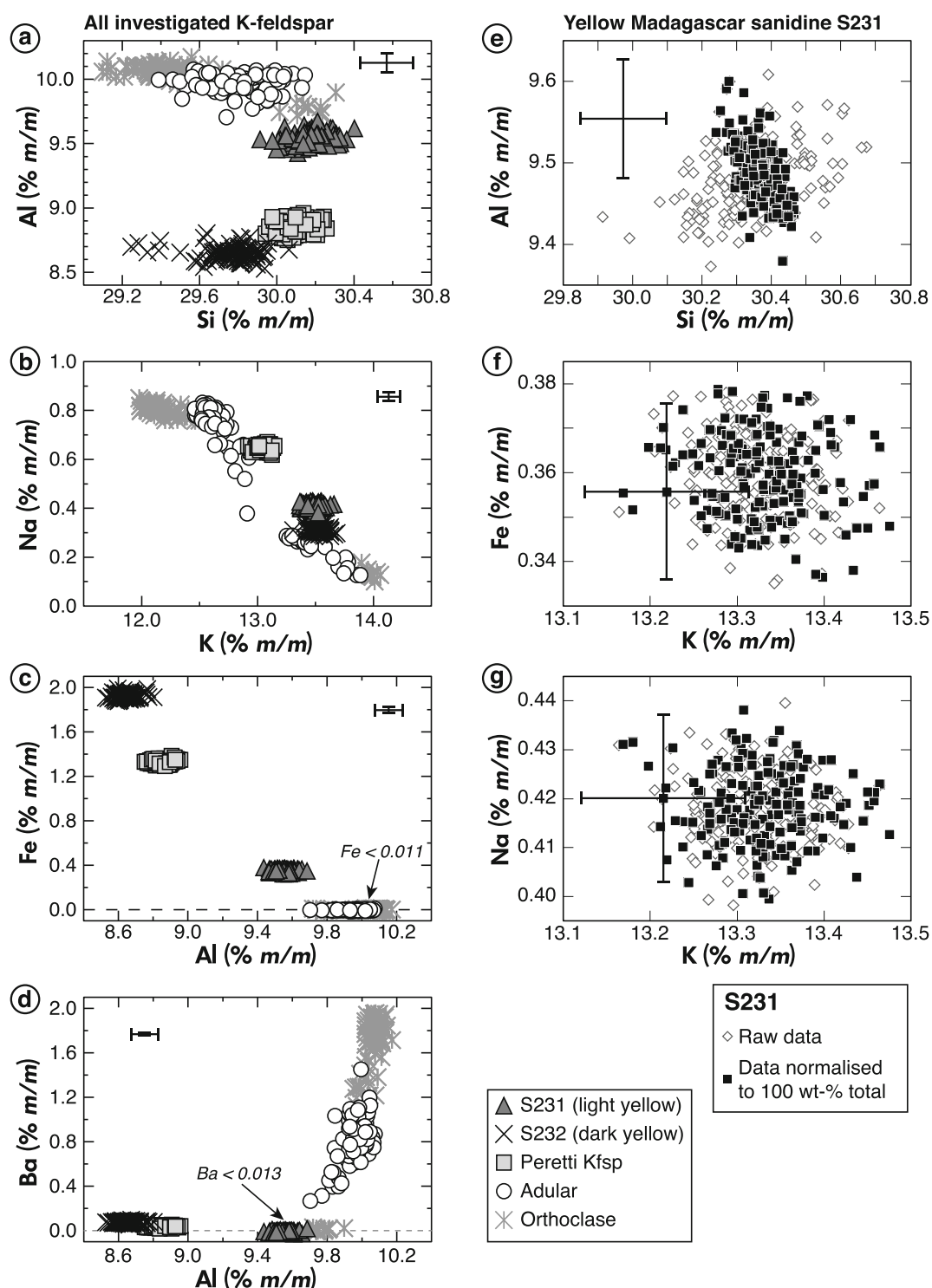There is no clear correlation between Ca, Na and K, yet a negative correlation is suggested between Si and Al % *m/m* when normalised to 100% (Figure 5b) and a slight positive correlation between Ca and Sr (Table S4). Nonetheless, both variations remain close to or below the analytical error of the respective element analysed, and the variation could also be attributed to the use of different µRM and matrix correction routines. All EPMA laboratories investigating this sample yield excellent results close to 100% totals and identical results within the analytical uncertainty of the respective instrument (which vary depending on beam conditions, counting time, spectrometer, background correction methods, etc., Table S2).

The level of homogeneity of Si, Al, Na, Ca and K in Piz Beverin albite was first tested using the homogeneity

Figure 9. Quantitative element maps in % *m/m* in K-feldspar samples S231, ETH Adular, and ETH Orthoclase acquired at 15 keV, 50 nA, 5 µm beam size, 50 ms per pixel dwell time, and using the spectrometer setup listed in Table 2c. Silicon was not determined and assumed homogeneous in each mineral. For matrix-correction purposes, Si-content was specified to the averaged % *m/m* value obtained by EPMA in each respective K-feldspar. The apparent lower Al-content on the top-right corner of sample S231 is due to spectrometer defocusing: this area was exceptionally large (> > 1 mm) and the polished sample surface was not flat enough, but rather dome-shaped towards the top-right corner, yielding unavoidable WD spectrometer artefact.

S231 (yellow sanidine)
4.49 × 8.47 mm

ETH Adula
1.635 × 2.61 mm

ETH Orthoclase
1) 3.85 × 1.86 mm
2) 0.6 × 0.426 mm

Al % *m/m*

K % *m/m*

Na % *m/m*

Fe % *m/m*

Ba % *m/m*

Figure 10. Quantitative EPMA analyses in all investigated K-feldspar samples. (a–d) All investigated K-feldspar samples and (e–g) detail of homogeneity test in S231. Homogeneity of S232 and Peretti Kfsp is similar to S231. All data are available in the Table S8. Cross on each plot represents the analytical uncertainties.

calculation available in Probe for EPMA using the first EPMA data obtained in PB0. This approach compares 99% confidence level (3s) of the data with an assumed 1%

relative variability in the absolute % m/m content. All major elements passed this test in the Piz Beverin albite. Evaluation of the repetitions of analysis and associated uncertainty is

Table 8.
LA-ICP-MS measurement results for sample S231

El.	Mass	Min	Max	% pt < DL	S231, all 117 pts	Line 1 58 pts	Line 2 59 pts
Si (% *m/m*)	29	28.85	29.62	0.0%	29.24	29.21	29.27
Al (IS)	-	-	-	-	9.48	9.48	9.48
K (% *m/m*)	39	12.38	12.85	0.0%	12.58	12.55	12.62
Values below in µg g^{-1}							
Na	23	4138	4335	0.0%	4210(40)	4220(40)	4200(30)
Fe	57	3330	4162	0.0%	3510(160)	3590(190)	3440(40)
Rb	85	220	231	0.0%	224.9(2.4)	224.1(2.2)	225.6(2.3)
Mg	24	184	227	0.0%	223(7)	221(9)	224.0(1.6)
B	11	81.0	380.1	0.0%	120(60)	130(80)	105(10)
Ba	137	76.9	126.7	0.0%	114(12)	112(14)	115(10)
Ti	49	29.8	45.2	0.0%	32.4(2.0)	32.9(2.6)	31.9(9)
Be	9	4.0	6.3	0.0%	4.7(3)	4.7(4)	4.63(21)
Zn	66	3.2	6.2	0.0%	3.6(3)	3.6(2)	3.6(4)
Sr	88	0.7	1.3	0.0%	1.12(12)	1.10(13)	1.13(9)
Cs	133	0.83	1.10	0.0%	1.00(6)	0.98(7)	1.02(5)
Pb	208	0.50	0.80	0.0%	0.71(6)	0.69(6)	0.73(5)
Sc	45	0.14	0.34	0.0%	0.22(4)	0.24(4)	0.21(4)
Mn	55	< 0.8	4.9	0.9%	3.4(7)	3.2(8)	3.6(6)
V	51	< 0.05	0.154	2.6%	0.093(22)	0.092(22)	0.094(23)
Nb	93	< 0.015	0.0	8.5%	0.006(5)	0.0082(7)	0.0045(16)
Y	89	< 0.0011	0.0077	25.6%	0.0037(15)	0.0042(17)	0.0034(11)
Ce	140	< 0.0005	0.089	28.2%	0.0031(10)	0.0018(8)	0.004(13)
Zr	90	< 0.0014	0.0833	37.6%	0.012(16)	0.019(20)	0.0047(20)
Eu	151	< 0.0005	0.0034	38.5%	0.0017(5)	0.0017(6)	0.0017(5)
Cu	65	< 0.04	0.1291	40.2%	0.076(21)	0.074(20)	0.078(21)

Column "% < DL" indicates the percentage of data points below detection limit.

checked using the Quality Factor (QF, Potts and Webb 2022; Tables 3, S3 and S4). All elements except Ca and K pass the QF test with values below or near unity for data from several labs (Table 3). A few laboratories yield a higher QF around 2 to 3, owing to a slightly larger standard deviation of the acquired data compared with the expected statistics. The data acquired with the MAN background correction (labs C, E and F) systematically yield a smaller uncertainty in the measurements and therefore a QF closer to 1. This suggests a much smaller measurement uncertainty associated with the X-ray bremsstrahlung correction by MAN background correction for major elements compared with two short off-peak acquisitions yielding bremsstrahlung intensity with higher uncertainties (Donovan *et al.* 2016).

Further investigation using quantitative element maps in the large grain mounts of PB1 and PB2 by EPMA revealed the presence of 20–50 µm-size sealed fractures that contain very low Ca content (< 100 µg g^{-1}) compared with the core domains, which reaches up to ~ 900 µg g^{-1} Ca (Figures 5c,d, 7). Similarly, K varies from ~ 60 to 250 µg g^{-1}, with lower values vaguely correlated with the Ca-poor sealed fractures (Table S4). These fractures are highlighted by a higher density of fluid inclusions and a lower panchromatic CL intensity. Abnormal and extremely rare higher Ca, Sr, or K contents (> 1000 µg g^{-1}) are more likely due to the presence of (sub-) micrometre inclusions of (Sr-rich) carbonate, mica or clay minerals (e.g., Figure 4d, e).

The LA-ICP-MS data confirm the homogeneous nature of Si, Na and Al, and the inhomogeneous distribution (at 10s to 100s µg g^{-1} level) of Ca, Sr and K, with absolute values varying between ~ 20–700, 65–475 and 45–150 µg g^{-1}, respectively (Table 4). Other elements detected are, in order of importance, Zn (from < 1 µg g^{-1} and locally up to 10–50 µg g^{-1}), Ba (0.5 to 8 µg g^{-1}), Mg (< 0.4 to 7 µg g^{-1}), Sc (< 0.14 to 0.5 µg g^{-1}), Pb and Be (0.02 to 0.8 µg g^{-1}) and some REE in the ng g^{-1} range (La, Ce, Eu; Table 4 and Tables S5 and S6). Apparent Cs and Rb mass fractions are near their respective detection limit (~ 0.1 µg g^{-1}). Iron and Mn are clearly at or below the µg g^{-1} level. Copper was detected on a few points but never exceeded 0.6 µg g^{-1}.

Lithium remains below 0.1 µg g^{-1} with minor exceptions up to ~ 3 µg g^{-1}. All other elements investigated remained below detection limit (B, P, Ti, V, Cr, Co, Ni, Cu, Ga, Y, Zr, Nb, REEs, Hf, Ta, W, Th and U; see Table S6).

Panchromatic CL images in PB1 reveal a patchwork of variation of light intensity (e.g., Figure 4b; full cm-sized sample in Figure S3). Whereas the darkest veins are clearly correlated with Ca-poor domains, the reason for the larger-scale variations of intermediate to bright CL intensity remains unclear. To assess if this variation is due to variation in trace elements composition, representative "dark" and "light" CL domains were selected and further analysed by LA-ICP-MS (Table S5, Figure S3). No obvious change in composition was observed (Table 4). The crystallographic orientation and twinning are most likely causing this large-scale change in CL intensity, as suggested in Finch *et al.* (2003).

The two XRF analyses in PB1 and PB2 further confirm the overall purity of the set of albite crystals. Determinations of Si, Al and Na in both PB1 and PB2 are very similar (within error) and match the results obtained by EPMA. Results from PB2 yield slightly lower totals, lower Al and Na contents, and higher Si content, which is likely due to the presence of minor quartz impurities. Mean Ca, K and Sr % *m/m* are identical to the averaged EPMA data. Therefore, when a significant sample size is considered (i.e., bulk analysis or multiple grain analyses), these elements can appear homogeneous with ~ 475 Ca, ~ 150 K and ~ 340 Sr µg g^{-1}. P is merely detected by XRF around 10–20 µg g^{-1} and could stem from very minor apatite inclusions (e.g., Figure 4c). Iron, Mn and Mg are confirmed to be low and commonly below the detection limit (~ 10 to 100 µg g^{-1}; Table 5).

A representative Raman spectrum obtained of PB1 albite at ETH Zürich is presented in Figure 8. The raw data of this spectrum are available in Table S7 and has been uploaded to the RRUFF database (ID R230008, https://rruff.info/R230008). The three peaks found at 290.9, 479.6 and 507.8 cm^{-1} are known to reflect the degree of Al-Si-ordering in albite (e.g., Freeman *et al.* 2008, Tribaudino *et al.* 2018). The observed difference of 28.2 cm^{-1} between 479.6 and 507.8 cm^{-1} points to a high degree of ordering (Tribaudino *et al.* 2018) and thus indirectly confirms the sample as low-albite.

K-feldspar minerals

All K-feldspar minerals were analysed by EPMA to assess homogeneity. The two clear crystals of "ETH Adular" and "ETH Orthoclase" appear to have relatively homogeneous domains of similar compositions, with slightly different Ba contents. Their mean composition in % *m/m* is around 10.0% Al_2O_3, 29.7% SiO_2, 12.5% K_2O, 0.7% Na_2O, and 0.8 or 1.5% BaO, respectively. Unfortunately, both contain large domains (> 100 µm) of significantly different and variable compositions in K-, Ba- and Na-contents (Table 7), especially near rims and more subtly across the grains (Figure 9). Even if this inhomogeneity is localised and could be avoided (if known), it is not ideal for a µRM as there is a high risk of finding individual grains or parts of grains within the mineral separate with a composition that substantially deviates from the reference value.

A potential K-feldspar µRM could one day be found in the yellow "Itrongay sanidine (orthoclase)" of Madagascar. Three distinct sets were investigated (S231, S232 and Peretti Kfsp). Each of them passes the homogeneity tests for Si, Al and K on EPMA analyses (Figure 10a–d) and yields a QF below or near unity (Table 7). Unfortunately, they each yield distinct K, Na and Fe contents, with Fe being dominantly Fe^{3+} and inversely correlated with Al (Figure 10c). The Fe-content is responsible for the yellow colouration with a darker honey-yellow colour in the Fe-richest sample S232 (1.92 ± 0.05% *m/m* Fe), intermediate colour in "Peretti Kfsp", and a lighter yellow colour for the Fe-poor sample S231 (0.36 ± 0.03% *m/m* Fe; Figures 2i, 9). As they are homogeneous, each individual batch could be an excellent µRM for Si, Al and K. Unfortunately, only 1 to 10 g of each sample are currently available and therefore this material cannot be made into an internationally available µRM.

Sample S231 was further investigated by LA-ICP-MS, as it was the sample with the lowest Fe- and highest K-content, homogeneous at the micrometre-scale, and available in the "largest" quantity (~ 10 g). LA-ICP-MS results summarised in Table 8 confirm the homogenous composition revealed by EPMA for Si and K (although inaccurate and rather low) and reveal significant amounts of Na (4210 ± 70 µg g^{-1}; QF ~ 2.4) and slightly inhomogeneous Fe at the 100s µg g^{-1} level (3330 to 4162 µg g^{-1}; QF ~ 3.3), both consistent with EPMA data. Other identified elements include Rb (225 ± 5 µg g^{-1}), Mg (223 ± 14), Ba (114 ± 24), Ti (32 ± 4), and traces of Be, Zn, Sr, Cs, Pb, Sc and Mn (< 5 µg g^{-1} each; Table 8 and Table S6). Iron cannot be considered as homogeneous and clearly shows zonation across the grain, as do other trace elements such as B, Ba and to some extent Na.

Concluding remarks

The hardware for X-ray microanalysis by ED and WD on SEM or EPMA and the related computer programs have

considerably improved in terms of stability, reliability, methodology, matrix corrections and ultimately the accuracy of the results. New μRMs need to now be more reliable, with more accurate certified data, so we can hope to break the 1% accuracy barrier. Among other elements, Na and K analyses suffer from the lack of suitable and trustable material available in large quantities and easily available at little (to no) cost.

The Piz Beverin albite appears to exceed the quality expected from a natural sample for its homogeneity in Si, Al and Na-content and its near purity; quality factors (Potts and Webb 2022) are very near or below 1, and its absolute composition is confirmed by nine independent EPMA laboratories. Nonetheless, analysts using this μRM should be aware of possible natural variation in the order of ± 0.5% relative Si or Al. This accuracy error mostly remains below the measurement uncertainty by EPMA, here estimated at ± 1% relative (2s) at the best. The absolute contents of Si, Al and Na at the sample scale are verified by XRF and close to what is delivered by the LA-ICP-MS. This agreement ascertains the low quantity of trace elements, with heterogeneous yet trace amounts of Ca, K and Sr. EPMA data remain however more accurate over LA-ICP-MS or XRF when it comes to major element determination. A consensus composition for the Piz Beverin albite recommended to be used by all laboratories using this μRM is given in the last column of Table 6, along with an atomic proportion recalculated out of eight oxygen atoms. This recommended value is based on a weighted mean of all EPMA laboratories using the standard deviation of each laboratory as the weighting factor, with an adjustment for the low Sr-content based on LA-ICP-MS data. Uncertainty is provided as a 2s standard error assuming nine repetitions (from the nine participating EPMA laboratories). Researchers interested in a fraction of the Piz Beverin albite should contact the first author or a committee member of FIGMAS (https://figmas.org).

Acknowledgements

Data availability statement

The authors confirm that the data supporting the findings of this study are available within the article and its supplementary materials.

References

Armstrong J.T. (1988)
Quantitative analysis of silicate and oxide materials: Comparison of Monte Carlo, ZAF and φ(ρz) procedures. In: Newbury D.E. (ed.), Microbeam analysis. San Francisco Press, 239–246.

Bullock E.S., Nachlas W., Neill O., Allaz J. and von der Handt A. (2021)
The FIGMAS online database of standards and reference materials – An update. Microscopy and Microanalysis, 27, 1572–1573.

Buse B. and Kearns S. (2015)
Importance of carbon contamination in high-resolution (FEG) EPMA of silicate minerals. Microscopy and Microanalysis, 21, 594–605.

Carpenter P.K. (2008)
EPMA standards: The good, the bad and the ugly. Microscopy and Microanalysis, 14, 530–531.

Carpenter P.K. and Vicenzi E.P. (2012)
Mineral reference standards and quantitative electron-probe microanalysis. Microscopy and Microanalysis, 18, 1734–1735.

Chantler C.T., Olsen K., Dragoset R.A., Chang J., Kishore A.R., Kotochigova S.A. and Zucker D.S. (2005)
X-ray form factor, attenuation and scattering tables (version 2.1). [Online]. National Institute of Standards and Technology (Gaithersburg, MD).

Coombs D.S. (1954)
Ferriferous orthoclase from Madagascar. Journal of The Mineralogical Society, 30, 409–427.

GEOSTANDARDS and GEOANALYTICAL RESEARCH

references

Donovan J.J., Allaz J.M., von der Handt A., Seward G.G.E., Neill O., Goemann K., Chouinard J. and Carpenter P.K. (2021)
Quantitative WDS compositional mapping using the electron microprobe. American Mineralogist, 106, 1717–1735.

Donovan J.J., Singer J. W. and Armstrong J.T. (2016)
A new EPMA method for fast trace element analysis in simple matrices. American Mineralogist, 101, 1839–1853.

Donovan J.J. and Tingle T.N. (1996)
An improved mean atomic number background correction for quantitative microanalysis. Journal of Microscopy and Microanalysis, 2, 1–7.

Drouin D., Couture A.R., Joly D., Tastet X., Aimez V. and Gauvin R. (2007)
CASINO V2.42 – A fast and easy-to-use modeling tool for scanning electron microscopy and microanalysis users. Scanning, 29, 92–101.

Finch A.A., Hole D.E. and Townsend P.D. (2003)
Orientation dependence of luminescence in plagioclase. Physics and Chemistry of Minerals, 30, 373–381.

Freeman J.J., Wang A., Kuebler K.E., Jolliff B.L. and Haskin L.A. (2008)
Characterization of natural feldspars by Raman spectroscopy for future planetary exploration. The Canadian Mineralogist, 46, 1477–1500.

Gunn J.S., Harrowfield I.R., Proctor C.H. and Thresher R.E. (1992)
Electron probe microanalysis of fish otoliths – Evaluation of techniques for studying age and stock discrimination. Journal of Experimental Marine Biology and Ecology, 158, 1–36.

Huebner S.J. and Woodruff M.E. (1985)
Chemical compositions and critical evaluation of microprobe standards available in the Reston Microprobe Facility. U.S. Geological Survey, Open-File Report 85–718, 237pp.

Ingamells C.O. (1981a)
Microprobe column. Geostandards Newsletter, 4, 253–254.

Ingamells C.O. (1981b)
Microprobe column. Geostandards Newsletter, 5, 101.

Ingamells C.O. (1981c)
Microprobe column. Geostandards Newsletter, 5, 195–196.

Ito J. and Frondel C. (1968)
Syntheses of the scandium analogues of aegirine, spodumene, andradite and melanotekite. American Mineralogist: Journal of Earth and Planetary Materials, 53, 1276–1280.

Jarosewich E. (2002)
Smithsonian microbeam standards. Journal of Research of the National Institute of Standards and Technology, 107, 681.

Jarosewich E., Nelen J.A. and Norberg J.A. (1980)
Reference samples for electron microprobe analysis. Geostandards Newsletter, 4, 43–47.

Potts P.J. and Webb P.C. (2022)
Simple test for the fitness for purpose of geological reference materials according to the uncertainties associated with their reference values. Geostandards and Geoanalytical Research, 46, 477–492.

Ribbe P.H. and Smith J.V. (1966)
X-ray-emission microanalysis of rock-forming minerals IV. Plagioclase feldspars. The Journal of Geology, 74, 217–233.

Simmons W.B. and Falster A.U. (2002)
Yellow orthoclase (sanidine) from South Betroka, Madagascar. Mineralogical Record, 33, 79.

Smith J.V. and Ribbe P.H. (1966)
X-ray-emission microanalysis of rock-forming minerals III. Alkali feldspars. The Journal of Geology, 74, 197–216.

Sperner B., Jonckheere R. and Pfänder J.A. (2014)
Testing the influence of high-voltage mineral liberation on grain size, shape and yield, and on fission track and $^{40}Ar/^{39}Ar$ dating. Chemical Geology, 371, 83–95.

Tribaudino M., Gatta G.D., Aliatis I., Bersani D. and Lottici P.P. (2018)
Al-Si ordering in albite: A combined single-crystal X-ray diffraction and Raman spectroscopy study. Journal of Raman Spectroscopy 49, 2028–2035.

Vicenzi E. and Rose T. (2008)
Hyperspectral X-ray analysis of submicrometer-scale heterogeneities in a venerable compositional standard provided by nature: Kakanui hornblende. Microscopy and Microanalysis, 14, 522–523.

Wyss R. and Wiederkehr M. (2017)
Geologischer Atlas der Schweiz - 1215 Thusis: Erläuterungen. Bundesamt für Landestopografie swisstopo, 110pp.

Supporting information

The following supporting information may be found in the online version of this article:

Figure S1. Variation of X-ray intensity in counts per second per nanoampere over time using various beam currents and beam sizes to assess the maximum beam dosage at a certain beam size.

Figure S2. Plots of EPMA measurement results obtained in all mounts of PB albite at ETH Zürich. (a) Quantitative EPMA analyses in PB1 and PB2 at 15 keV. (b, c) EPMA analyses of mineral separate of clear and milky crystals in PB1 fraction 0.5–1.0 mm and PB2 fraction 1–2 mm at 10 keV.

Figure S3. Backscattered electron and panchromatic cathodoluminescence images in a single cm-sized albite sample (PB1).

Table S1. Wavelength dispersive scan in PB1 on LDE1, TAP, TAP-H, PET-L and LiF-H monochromators at 15 keV, 100 nA, 20 μm beam size, 50 μm step, 500 ms (or 600 ms on H-type), full range scan.

Table S2. Simplified analytical conditions of each EPMA instruments involved in the evaluation of the PB albite microanalytical RM.

Table S3. Complete set of EPMA measurement results obtained at ETH Zürich on all mounts of PB0 (see also Table 3, lab F), PB1 and PB2.

Table S4. EPMA measurement results from the nine independent laboratories.

Table S5. Complete set of LA-ICP-MS measurement results at ETH Zürich in cm-sized PB1 and PB2 grain mounts.

Table S6. List of elements measured by LA-ICP-MS or XRF that were found to be mostly or all below the detection limit.

Table S7. Raw Raman data expressed as wavenumber (cm^{-1}) versus intensity in arbitrary units.

Table S8. Complete set of EPMA data for candidate K-feldspar microanalytical reference materials: Yellow sanidine from Madagascar (a) S231 (1st grain mount), (b) S231 (2nd grain mount), (c) S232, (d) A. Peretti sample, (e) ETH orthoclase and (f) ETH adular.

This material is available from: http://onlinelibrary.wiley.com/doi/10.1111/ggr.12515/abstract (This link will take you to the article abstract).